

A BAYESIAN PANEL VECTOR AUTOREGRESSION TO ANALYZE THE IMPACT OF CLIMATE SHOCKS ON HIGH-INCOME ECONOMIES

BY FLORIAN HUBER^{1,a}, TAMÁS KRISZTIN^{2,1,b} AND MICHAEL PFARRHOFER^{3,c}

¹*Department of Economics, University of Salzburg, florian.huber@plus.ac.at*

²*Integrated Biosphere Futures Group, International Institute for Applied Systems Analysis (IIASA), krisztin@iiasa.ac.at*

³*Department of Economics, University of Vienna, michael.pfarrhofer@univie.ac.at*

In this paper we assess the impact of climate shocks on futures markets for agricultural commodities and a set of macroeconomic quantities for multiple high-income economies. To capture relations among countries, markets, and climate shocks, this paper proposes parsimonious methods to estimate high-dimensional panel vector autoregressions. We assume that coefficients associated with domestic lagged endogenous variables arise from a Gaussian mixture model while further parsimony is achieved using suitable global-local shrinkage priors on several regions of the parameter space. Our results point toward pronounced global reactions of key macroeconomic quantities to climate shocks. Moreover, the empirical findings highlight substantial linkages between regionally located shocks and global commodity markets.

1. Introduction. A projected increase in extreme climate events and an increasingly interdependent food supply chain pose a threat to global food security. Increasing trade flows and the rising complexity of economic networks may lead to higher vulnerability and systemic disruptions (Puma et al. (2015)). Isolating the effects of climate-related production shocks on agricultural commodity markets, food prices, and the globalized economy is thus of special interest to policy makers and the wider public in general. For instance, major central banks, such as the European Central Bank, now explicitly address climate change in the conduct of their monetary policies.

Global commodity markets play a crucial role in establishing a relationship between agricultural production and the economy. Due to increased demand and limited production capabilities, volatilities associated with agricultural prices are expected to rise over the next decades (FAO (2017), IFPRI (2008)). Among the key drivers of increasing volatility in related prices are exogenous weather and production shocks as well as influences from other economic sectors (e.g., demand, energy market, and exchange rate market shocks, see, for instance, Gilbert (2010), Nazlioglu (2011), Nazlioglu and Soytaş (2012), Serra et al. (2011)). Relatedly, changes in fiscal and monetary policies affect food price volatility (Akram (2009), Baffes and Haniotis (2010)).

Besides an overall trend toward increased volatilities in commodity prices, linkages across agricultural and energy markets strengthened in recent years, for instance, due to the rising importance of biofuels. The literature shows that this results in intensified competition for food production resources (see Enders and Holt (2014), Harri, Nalley and Hudson (2009), Nazlioglu and Soytaş (2011), Saghalian (2010), Havlík et al. (2011)). And such linkages are expected to strengthen further as a consequence of climate change. This in turn calls for research on the effects of climate shocks and their respective impact on real and financial economic sectors across economies, with a special focus on food prices, and feedback and spillover effects between countries (Gilbert (2010), Jebabli, Arouri and Teulon (2014)).

Received October 2021; revised July 2022.

Key words and phrases. Climate change impacts, commodity markets, food security, hierarchical modeling, factor stochastic volatility models, second keyword.

International trade is not only generally perceived as an important mitigation mechanism of economic fluctuations but also as another potential source of volatility (Gaupp et al. (2017), Hirsch, Krisztin and See (2020), Huang, von Lampe and van Tongeren (2011), Janssens et al. (2020), Sandström et al. (2018)). Addressing cross-country interdependencies on the macrolevel is crucial, especially when aiming to capture the international effects of climate shocks in highly globalized markets. The vast majority of the literature on volatility transmissions from climate change on agricultural markets and food security, however, neglects such notions and, instead, focuses solely on the nexus between global commodity markets and climate shocks (see, e.g., Enders and Holt (2014), Garcia, Irwin and Smith (2015), Harri, Nalley and Hudson (2009), Nazlioglu and Soytas (2011)). Such approaches disregard the fact that global commodity prices do not capture country-specific movements in food prices, which might depart considerably from global dynamics. Apart from considering global commodity markets, studies focusing on the impact of climate-related shocks on country-specific macroeconomic and commodity market-related quantities typically fail to take potential spillovers or feedback effects from trade, exchange rates, and other global factors into account (see, e.g., Guerrero, Hernández-del Valle and Juárez-Torres (2017), van Huellen (2018)).

These shortcomings thus call for a multicountry setup that takes cross-country spillovers and feedback effects between economies into account explicitly. Popular large-scale macroeconomic models, however, are typically heavily parameterized. This often leads to imprecise inference, rendering policy relevant conclusion difficult. From a methodological point of view, the main contribution of this paper is to propose a parsimonious yet flexible approach to estimate panel vector autoregressive (PVAR) models. We combine the literature on Bayesian PVAR models (see Canova and Ciccarelli (2004), Feldkircher et al. (2022), Canova and Ciccarelli (2009), Koop and Korobilis (2016), Korobilis (2016)) with the literature on finite mixture models (see Allenby, Arora and Ginter (1998), Lenk and DeSarbo (2000), Frühwirth-Schnatter, Tüchler and Otter (2004), Frühwirth-Schnatter and Kaufmann (2008), Malsiner-Walli, Frühwirth-Schnatter and Grün (2016), Hauenberger et al. (2021)). Dependency structures across economies are pushed to zero by means of global-local shrinkage priors in the spirit of Griffin and Brown (2010) and Huber and Feldkircher (2019). To account for international co-movement of volatilities that vary over time, we assume that the errors of the system feature a factor stochastic volatility structure. This provides a parsimonious representation for a high-dimensional time-varying variance-covariance matrix (see Kastner (2019a), Kastner and Huber (2020)).

The empirical contribution deals with the question of how climate shocks impact country-specific macroeconomic fundamentals. Our approach is differentiated from other related papers that assess climate impacts on the economy (e.g., Alessandri and Mumtaz (2021), Kim, Matthes and Phan (2021)) in that we specifically attempt to trace the impact through the channels of agricultural production and commodity markets. To control for international movements in commodity markets, our baseline model features a global block, which consists of commodity futures data from the United States (U.S.), and is akin to the framework proposed in Georgiadis (2015). In addition, we jointly model 17 OECD economies, where each country-specific model features several key macroeconomic variables alongside food prices. We specifically focus on high-income developed economies to: (1) demonstrate the impact of climate change on the macroeconomy of countries whose agricultural production constitutes only a small part of output, and thus direct feedback from the agricultural sector is low; (2) our selection of countries is motivated by our proposed methods requiring a balanced panel dataset with a sufficiently large number of observations. Moreover, as both climate shocks and commodity markets exhibit faster movements than the usual quarterly modeling framework, we choose to use data on a monthly frequency. This further constrains our selection of economies.

Another empirical contribution of this paper is the development of an index to measure climate shocks impacting the agricultural sector. Our proposed index has the virtue of attempting to isolate climate-related shocks to the agricultural sector by focusing on specifically agriculture-related climate risks that impact a large part of global food production and hence significantly endanger food security (as opposed to more localized damage). In our modeling framework, climate shocks, assessed in terms of agricultural production under risk of drought or flooding/excessive rainfall in 11 global regions are treated as strictly exogenous. Our results demonstrate that climate shocks have a substantial impact on short-term interest rates and inflation—the primary conventional policy tool and target variable of central banks—and, to a lesser degree, on output and exchange rates. Significant impacts are present, even if the regions hit by climate shocks are neither in the countries themselves nor among major trading partners, likely due to the integration of global financial markets.

The paper is structured as follows. Section 2 introduces the general econometric framework and specifies the adopted prior setup. We proceed by introducing the novel dataset in Section 3. This section also includes further details on the model specification. The empirical findings are discussed in Section 4. The last section summarizes and concludes the paper. Additional empirical results, robustness checks and simulation-based evidence are provided in the Supplementary Material (Huber, Krisztin and Pfarrhofer (2023)).

2. Econometric framework. In this section we discuss the PVAR model along with important specification issues in Section 2.1, while the remainder of the section is devoted to dealing with these issues using flexible Bayesian shrinkage priors. Before proceeding to the model, it is convenient to introduce generic notation. In what follows, capitalized letters without a time index refer to full-data matrices, that is, $\mathbf{Y} = (\mathbf{y}_1, \dots, \mathbf{y}_T)'$, unless otherwise noted. The notation $[\mathbf{Y}]_{j\bullet}$ selects the j th row of the matrix \mathbf{Y} while $[\mathbf{Y}]_{\bullet j}$ selects its j th column. In addition, we let $\mathbf{y}_{-i,t}$ denote the vector \mathbf{y}_t with the i th subvector excluded, that is, $\mathbf{y}_{-i,t} = (\mathbf{y}'_{1t}, \dots, \mathbf{y}'_{i-1t}, \mathbf{y}'_{i+1t}, \dots, \mathbf{y}'_{Nt})'$. Finally, we let \bullet be a generic notation that indicates conditioning on all remaining coefficients in the model as well as the data.

2.1. The panel vector autoregressive model. In this paper we aim to model a set of M macroeconomic and financial variables across a set of N countries. For each country the domestic quantities are stored in an M -dimensional vector \mathbf{y}_{it} for $i = 1, \dots, N$ and $t = 1, \dots, T$, subsequently stacked in a vector $\mathbf{y}_t = (\mathbf{y}'_{1t}, \dots, \mathbf{y}'_{Nt})'$ of dimension $K = MN$. We assume that \mathbf{y}_{it} follows a vector autoregressive (VAR) process:

$$(1) \quad \mathbf{y}_{it} = \boldsymbol{\beta}_i + \mathbf{A}_{i1}\mathbf{y}_{it-1} + \dots + \mathbf{A}_{iP}\mathbf{y}_{it-P} + \mathbf{B}_{i1}\mathbf{y}_{-i,t-1} + \dots + \mathbf{B}_{iP}\mathbf{y}_{-i,t-P} + \boldsymbol{\varepsilon}_{it},$$

where $\boldsymbol{\beta}_i$ is an M -dimensional intercept vector and \mathbf{A}_{ij} ($j = 1, \dots, P$) denotes a set of $M \times M$ -dimensional coefficient matrices associated with the P lags of \mathbf{y}_{it} . In what follows, we label these parameters the domestic VAR coefficients. The impact of other countries' lagged dependent variables $\mathbf{y}_{-i,t-j}$ is measured through the matrices \mathbf{B}_{ij} which are of dimension $M \times (N - 1)M$.

Equation (1) can be cast in the usual regression form

$$(2) \quad \mathbf{y}_{it} = \mathbf{C}_i\mathbf{x}_{it} + \mathbf{B}_i\mathbf{x}_{-i,t} + \boldsymbol{\varepsilon}_{it},$$

with $\mathbf{x}_{it} = (1, \mathbf{y}'_{it-1}, \dots, \mathbf{y}'_{it-P})'$, $\mathbf{C}_i = (\boldsymbol{\beta}_i, \mathbf{A}_{i1}, \dots, \mathbf{A}_{iP})$, $\mathbf{x}_{-i,t} = (\mathbf{y}'_{-i,t-1}, \dots, \mathbf{y}'_{-i,t-P})'$, and $\mathbf{B}_i = (\mathbf{B}_{i1}, \dots, \mathbf{B}_{iP})'$. The matrix \mathbf{B}_i establishes dynamic interdependencies (DIs) between countries i and j . In the literature on PVAR models (see Canova and Ciccarelli (2013), for a recent survey), an important modeling decision is whether to set certain submatrices of \mathbf{B}_i to zero, shutting off dynamic relations between country pairs. An extreme version of the

model would set the whole matrix \mathbf{B}_i to zero, ruling out lagged relations between country i and the remaining economies.

Up to this point, we remained silent on assumptions regarding error covariances across countries. Here, we stack the country-specific errors $\boldsymbol{\varepsilon}_{it}$ in a K -dimensional vector $\boldsymbol{\varepsilon}_t = (\boldsymbol{\varepsilon}'_{1t}, \dots, \boldsymbol{\varepsilon}'_{Nt})'$ and assume that

$$(3) \quad \boldsymbol{\varepsilon}_t \sim \mathcal{N}(\mathbf{0}, \boldsymbol{\Sigma}_t),$$

where $\boldsymbol{\Sigma}_t$ is a full $K \times K$ -dimensional variance covariance matrix.

High-dimensional PVAR models, such as the one proposed in equations (1) to (3), are highly parameterized, and model uncertainty is pervasive. Three important dimensions of model uncertainty have been identified by the literature. The first one is concerned with modeling contemporaneous relations across the shocks in the system (called static interdependencies, SIs), while the second dimension centers on the question whether coefficients associated with lagged domestic variables are homogeneous across countries (labeled homogeneity restrictions). If such domestic coefficients are similar, so-called homogeneity restrictions might be imposed, effectively introducing the same set of coefficients for several countries and, therefore, reducing the number of free parameters. The final dimension deals with the question on whether to allow for lagged dependencies between countries (labeled dynamic interdependencies, DIs).

Considering the recent literature on model specification and selection in PVAR models reveals two commonly used approaches to deal with the aforementioned issues. The first strand of the literature suggests applying shrinkage priors to stochastically select an appropriate model specification (see [Koop and Korobilis \(2016\)](#), [Korobilis \(2016\)](#)). In light of the large number of potential restrictions, however, mixing issues typically arise, leading to weak convergence properties of existing algorithms ([Bhattacharya et al. \(2015\)](#)). The second strand considers additional restrictions that reduce the dimension of the parameter space. For instance, [Canova and Ciccarelli \(2009\)](#) assume that the (time-varying) coefficients of their PVAR model feature a factor structure. This translates into statistical and computational gains since the dimension of the state space is substantially reduced. Another prominent example are global VAR models (see, e.g., [Dees et al. \(2007\)](#), [Pesaran, Schuermann and Weiner \(2004\)](#), [Feldkircher and Huber \(2016\)](#), [Crespo Cuaresma, Feldkircher and Huber \(2016\)](#), [Huber \(2016\)](#)) that introduce parametric restrictions on the coefficients associated with other countries' endogenous variables.

2.2. Dealing with static interdependencies. In this section we start with discussing how to tackle the first dimension of model uncertainty. SIs are introduced by using a factor stochastic volatility structure ([Kastner \(2019a\)](#), [Pitt and Shephard \(1999\)](#), [Aguilar and West \(2000\)](#)) on $\boldsymbol{\Sigma}_t$,

$$(4) \quad \boldsymbol{\Sigma}_t = \mathbf{L}\mathbf{H}_t\mathbf{L}' + \boldsymbol{\Omega}_t.$$

\mathbf{L} is a $K \times q$ matrix of factor loadings (with $q \ll K$), $\mathbf{H}_t = \text{diag}(e^{h_{1t}}, \dots, e^{h_{qt}})$ is a diagonal matrix containing the variances of a set of q common factors $\mathbf{f}_t \sim \mathcal{N}(\mathbf{0}, \mathbf{H}_t)$, and $\boldsymbol{\Omega}_t = \text{diag}(e^{\omega_{1t}}, \dots, e^{\omega_{Kt}})$ is a diagonal variance-covariance matrix of idiosyncratic shocks $\boldsymbol{\eta}_t \sim \mathcal{N}(\mathbf{0}, \boldsymbol{\Omega}_t)$. The factors in \mathbf{f}_t can be latent or observed. In our empirical work we construct exogenous climate shock measures and include these shocks as observed factors in our model.

An equivalent representation of equation (4) is the regression form

$$\boldsymbol{\varepsilon}_t = \mathbf{L}\mathbf{f}_t + \boldsymbol{\eta}_t.$$

The key feature from a computational point of view is that conditional on $\mathbf{L}\mathbf{f}_t$, the PVAR reduces to a system of unrelated regression models. This leads to substantial computational

gains relative to full system estimation (see [Kastner and Huber \(2020\)](#), for more details and an efficient algorithm). More importantly, the resulting estimation approach will be order-invariant (see [Chan, Eisenstat and Yu \(2022\)](#)), different to many recent estimation algorithms in the spirit of [Carriero, Clark and Marcellino \(2019\)](#).

We assume that the (log) of the main diagonal elements of \mathbf{H}_t and $\mathbf{\Omega}_t$ follow independent AR(1) processes:

$$(5) \quad h_{jt} = \rho_{hj} h_{jt-1} + \sigma_{hj} \zeta_{hj,t}, \quad \text{for } i = 1, \dots, q,$$

$$(6) \quad \omega_{jt} = \phi_{\omega j} + \rho_{\omega j} (\omega_{jt-1} - \phi_{\omega j}) + \sigma_{\omega j} \zeta_{\omega j,t}, \quad \text{for } j = 1, \dots, K.$$

We let $\phi_{\omega j}$ denote the unconditional mean of the log-volatility, ρ_{sj} the autoregressive parameter, and σ_{sj}^2 the process innovation variance for $s \in \{h, \omega\}$. Moreover, $\zeta_{sj,t} \sim \mathcal{N}(0, 1)$ is a serially uncorrelated white noise shock. To identify the unconditional scaling of the factors, equation (5) is assumed to have zero mean.

As opposed to $K(K+1)/2$ total parameters in the case of an unrestricted $\mathbf{\Sigma}_t$, the structure in equation (4) implies that we only have to estimate $(K+1)q + K$ coefficients, a substantial reduction relative to an unrestricted variance-covariance matrix if q is small. One important consequence of equation (4) is that the covariance structure of the errors is driven by relatively few latent factors that summarize the joint dynamics of $\mathbf{\varepsilon}_t$. This assumption is warranted by the fact that macroeconomic data are often driven by a relatively low number of fundamental shocks (see, e.g., [Bai and Ng \(2007\)](#)).

2.3. Dealing with parameter homogeneity. It is worth noting that the total number of parameters of the PVAR model, outlined in the previous section, is $K(pK+1) + (K+1)q + K$ and thus rises rapidly with K (and implicitly with M and N). Since typical macroeconomic datasets include time series with only a few hundred observations, some form of regularization is needed. To cope with this issue, the Bayesian literature suggested various means of achieving parsimony in the PVAR framework. One strand of the literature uses shrinkage priors on several parts of the parameter space ([Koop and Korobilis \(2016\)](#), [Korobilis \(2016\)](#), [Koop and Korobilis \(2018\)](#)). This approach conceptually treats the PVAR as a large VAR with asymmetric shrinkage on the different coefficients in \mathbf{A}_i , \mathbf{B}_i , and the free elements in $\mathbf{\Sigma}_t$. Another strand ([Canova and Ciccarelli \(2004\)](#), [Canova and Ciccarelli \(2009\)](#), [Jarociński \(2010\)](#)) exploits the observation that countries do not differ much in terms of their domestic macroeconomic dynamics, implying that the matrices \mathbf{A}_i tend to be similar across countries. This literature often pools information across countries by shrinking toward a common mean of \mathbf{A}_i but neglects dynamic or static interdependencies.

We deal with the second pillar of model uncertainty (parameter homogeneity across countries) by assuming that the domestic coefficients $\mathbf{c}_i = \text{vec}\{\mathbf{C}_i\}$ arise from a G -component mixture of Gaussians distribution. A variant of this model has been proposed in the marketing literature ([Allenby, Arora and Ginter \(1998\)](#), [Lenk and DeSarbo \(2000\)](#), [Frühwirth-Schnatter, Tüchler and Otter \(2004\)](#)) and is commonly referred to as the heterogeneity model. In the present framework the mixture distribution for \mathbf{c}_i is given by

$$(7) \quad p(\mathbf{c}_i | \mathbf{w}, \boldsymbol{\mu}_1, \dots, \boldsymbol{\mu}_G, \mathbf{V}) = \sum_{g=1}^G w_g f_{\mathcal{N}}(\mathbf{c}_i | \boldsymbol{\mu}_g, \mathbf{V}).$$

Here, $\mathbf{w} = (w_1, \dots, w_G)'$ is a vector of component weights that satisfy $\sum_{g=1}^G w_g = 1$ and $w_g \geq 0$. Additionally, $f_{\mathcal{N}}$ is the density of the multivariate Gaussian distribution, $\boldsymbol{\mu}_g$ is an $m = M(Mp+1)$ -dimensional component-specific mean vector, and \mathbf{V} is a common variance-covariance matrix. This specification assumes that coefficients of countries within a given country group tend to be similar, with potential deviations from $\boldsymbol{\mu}_g$ driven by \mathbf{V} .

To estimate the mixture model, we introduce a set of N parameters δ_i that allow to state equation (7) as

$$p(\mathbf{c}_i | \delta_i = g, \boldsymbol{\mu}_g, \mathbf{V}) = f_{\mathcal{N}}(\mathbf{c}_i | \boldsymbol{\mu}_g, \mathbf{V}),$$

with $\Pr(\delta_i = g) = w_g$. In what follows, we exploit this auxiliary representation for estimation of the mixture model. Notice that ergodic averages of the posterior draws¹ of δ_i can be used to obtain the probability that country i is located within a specific country group.

On the main diagonal elements of \mathbf{V} , we apply a set of independent inverted Gamma priors,

$$v_j \sim \mathcal{G}^{-1}(w_0, w_1), \quad \text{for } j = 1, \dots, m,$$

with the hyperparameters w_0 and w_1 typically set to small values, that is, $w_0 = w_1 = 0.01$. This leads to a weakly informative prior on the common variances.

Another key assumption is that each mixture component again comes from a common distribution,

$$\boldsymbol{\mu}_g | \boldsymbol{\mu}_0, \mathbf{Q}_0 \sim \mathcal{N}(\boldsymbol{\mu}_0, \mathbf{Q}_0) \quad \text{for } g = 1, \dots, G.$$

We let $\boldsymbol{\mu}_0$ denote a common mean, and \mathbf{Q}_0 is a diagonal variance-covariance matrix that can be decomposed as

$$\mathbf{Q}_0 = \boldsymbol{\Lambda} \mathbf{R}_0 \boldsymbol{\Lambda},$$

where the matrix $\boldsymbol{\Lambda} = \text{diag}(\sqrt{\lambda_1}, \dots, \sqrt{\lambda_m})$ contains the standard deviations and $\mathbf{R}_0 = \text{diag}(R_1^2, \dots, R_m^2)$ constitutes an additional scaling matrix with R_j^2 denoting the range of $\mathbf{c} = (\mathbf{c}_1, \dots, \mathbf{c}_N)$ along the j th dimension (see Malsiner-Walli, Frühwirth-Schnatter and Grün (2016)).

Standard shrinkage priors force the coefficients toward the origin. By contrast, our shrinkage prior borrows strength from parameter estimates of other countries' domestic dynamics. Hence, if the parameters \mathbf{c}_i are similar for a selected group of countries, our prior groups them together and, by estimating a group-specific mean parameter, captures the notion that several regions of the parameter space should be very similar (but not identical). In large panels this approach has the substantial advantage that the resulting coefficient matrix (which is possibly huge dimensional if N is large) will not be sparse and the effective dimension of the state space is reduced. This has the immediate effect that, in light of heavy shrinkage, impulse responses within a given country group will be similar but nonzero. By contrast, in the case of a standard shrinkage prior, which pulls all elements to zero, the corresponding responses will be centered on zero.²

Selecting cluster-relevant quantities. To select the driving forces behind cluster allocation, we follow Yau and Holmes (2011) and consider the standardized distance between cluster centers for a given element j of $\boldsymbol{\mu}_i$ for clusters g and s ,

$$\frac{(\mu_{gj} - \mu_{sj})}{\sqrt{2R_j^2}} \sim \mathcal{N}(0, \lambda_j) \quad \text{for } j = 1, \dots, m.$$

¹This is based on classic Bayesian sampling theory, where the ergodic theorem is used to demonstrate that the ergodic averages of the posterior draws converge in probability to the posterior mean under the assumption of stationarity.

²In this case, only impact reaction will differ from zero, under the assumption that the factor loadings \mathbf{L} are nonzero.

By specifying a suitable mixing density on λ_j , we can flexibly shrink the distance between cluster centers to zero and thus are able to identify cluster relevant variables. As an example, consider a situation where the conditional mean of output growth strongly differs across countries while the remaining quantities (i.e., the coefficients associated with the lags of y_{it}) display only minor differences. In such a situation a shrinkage prior would strongly pull the cluster centers together for elements in μ not related to the intercept, while, at the same time, allowing for large differences between the cluster means for the intercept terms.

Following Malsiner-Walli, Frühwirth-Schnatter and Grün (2016), we introduce a Gamma prior on λ_j , leading to a variant of the Normal–Gamma (NG) shrinkage prior (Griffin and Brown (2010)). More specifically, we set

$$\lambda_j \sim \mathcal{G}(v_1, v_2),$$

where v_1 and v_2 are hyperparameters specified by the researcher. Notice that if $v_1 = 1$, we obtain the Bayesian Lasso (Park and Casella (2008)) used in Yau and Holmes (2011). The NG prior improves upon the Lasso by featuring a marginal prior that possesses heavier tails than the Laplace distribution. In fact, the marginal prior of the proposed specification is available in closed form (Frühwirth-Schnatter (2011)),

$$(8) \quad p(\mu_{1j}, \dots, \mu_{Gj} | \mu_0) = \frac{v_2^{v_1}}{(2\pi)^{G/2} \Gamma(v_1)} 2K_{p_G}(\sqrt{d_j} e_j) \left(\frac{e_j}{d_j}\right)^{p_G/2},$$

with $d_j = 2v_2$, $p_G = v_j - G/2$, $e_j = \sum_{g=1}^G (\mu_{gj} - \mu_{0j})^2 / R_j^2$, $\Gamma(\star)$ is the Gamma function, $K_\alpha(\star)$ represents the modified Bessel function of the second kind, and μ_{0j} denotes the j th element of μ_0 . Griffin and Brown (2010) show that the excess kurtosis of the NG prior is given by $3/v_1$ and thus rises with smaller values of v_1 . If v_1 is close to zero, more mass is placed on zero while, at the same time, heavy tails of the marginal prior are maintained. In the applications we specify $v_1 = v_2 = 1/2$ to strongly push the standardized distance between cluster centers to zero.

The prior on $\mu_0 \sim \mathcal{N}(\mathbf{m}_0, \mathbf{M}_0)$ is improper with \mathbf{m}_0 denoting the median over the columns of \mathbf{c} and $\mathbf{M}_0^{-1} = \mathbf{0}$. Here, one alternative would be to use a Minnesota prior (Doan, Litterman and Sims (1984)) at the top level of the hierarchy, assuming that μ_0 again features a normally distributed prior centered on a multivariate random walk with a known prior variance-covariance matrix. For several datasets, however, we found that this choice only exerts a minor impact on the results.

Choosing the number of mixture components. To endogenously select the number of components G , we follow Malsiner-Walli, Frühwirth-Schnatter and Grün (2016) and introduce a symmetric Dirichlet prior on the mixture component weights \mathbf{w} ,

$$\mathbf{w} \sim \text{Dir}(p_0, \dots, p_0),$$

where p_0 denotes the intensity parameter of the Dirichlet distribution. In the framework of overfitting mixture models (i.e., models that set G greater than the true number of clusters, G^{true}), the parameter p_0 plays an important role in shaping the way the algorithm treats redundant mixture components.³

In what follows, we place another Gamma prior on p_0 . Following Ishwaran, James and Sun (2001) and Malsiner-Walli, Frühwirth-Schnatter and Grün (2016), we choose a Gamma prior with expectation $E(p_0) = 1/G$,

$$p_0 \sim \mathcal{G}(c_0, c_0 G).$$

³For a discussion, see Frühwirth-Schnatter (2006) and Rousseau and Mengersen (2011).

Here, we let c_0 be a hyperparameter that controls the variance of the prior $1/(c_0G^2)$. This choice handles irrelevant mixture components by shrinking the associated weights to zero and empties superfluous components. Consistent with simulation evidence, provided in [Malsiner-Walli, Frühwirth-Schnatter and Grün \(2016\)](#), we set $c_0 = 10$.

2.4. Dealing with dynamic interdependencies. To decide on whether DIs, the third aspect of model uncertainty in PVARs, for a given country i are present, we use a NG shrinkage prior similar to the one discussed above. While the prior on μ_0 introduces local shrinkage parameters that push the differences between cluster centers toward zero, the standard implementation of the NG prior combines local shrinkage parameters with a global shrinkage factor that pulls all coefficients concerned to zero.

To illustrate the problem of selecting DIs, we partition the matrices \mathbf{B}_{ip} for $p = 1, \dots, P$ and stack them to obtain

$$\mathbf{B}_p = \begin{pmatrix} \mathbf{B}_{1p} \\ \mathbf{B}_{2p} \\ \vdots \\ \mathbf{B}_{Np} \end{pmatrix} = \begin{pmatrix} \mathbf{B}_{12,p} & \mathbf{B}_{13,p} & \dots & \mathbf{B}_{1N,p} \\ \mathbf{B}_{21,p} & \mathbf{B}_{23,p} & \ddots & \vdots \\ \vdots & \ddots & \vdots & \mathbf{B}_{N-1N,p} \\ \mathbf{B}_{N1,p} & \dots & \mathbf{B}_{NN-2,p} & \mathbf{B}_{NN-1,p} \end{pmatrix},$$

where the submatrix $\mathbf{B}_{ij,p}$ measures the DIs between countries i and j for lag p . Model specification boils down to deciding whether a given $\mathbf{B}_{ij,p}$ equals zero, ruling out DIs between countries i and j . [Koop and Korobilis \(2016\)](#) use a stochastic search variable selection (SSVS) prior that is based on a set of auxiliary measures that determine whether different submatrices of \mathbf{B}_p are pushed to zero. While this approach is conceptually straightforward to implement, a high-dimensional model space needs to be explored. Using MCMC techniques helps to circumvent this issue by performing a stochastic model specification search that only explores a fraction of the full model space. However, in large dimensions the possible number of DI restrictions is huge, even for a moderate number of countries included. In that case, even SSVS priors manage to exploit only a tiny fraction of the model space, leading to weak convergence (see [Bhattacharya et al. \(2015\)](#), for details).

In this paper we assume that each element of $\text{vec}(\mathbf{B}_i)$, labeled b_{ij} , features a normally distributed prior,

$$(9) \quad b_{ij} | \tau_{ij}, \xi_i \sim \mathcal{N}\left(0, \frac{2\tau_{ij}^2}{\xi_i}\right), \quad \tau_{ij}^2 \sim \mathcal{G}(\vartheta_i, \vartheta_i), \quad \xi_i \sim \mathcal{G}(c_0, c_1),$$

for $j = 1, \dots, k = PM^2(N - 1)$ and $i = 1, \dots, N$. ξ_i denotes a country-specific global scaling parameter that pushes all elements in \mathbf{B}_i (or, equivalently, \mathbf{B}_{ip} for all p) to zero, shutting off DIs between a given country and all remaining countries, if necessary. Overall shrinkage is driven by the hyperparameters c_0, c_1 , with small values translating into heavy shrinkage.

Since shutting of all DIs within a given country would be overly restrictive, we introduce a set of local scaling parameters τ_{ij}^2 . The local scaling parameters allow for nonzero b_{ij} 's, even in the presence of strong global shrinkage due to a heavy tailed marginal prior (see equation (8)), with excess kurtosis depending on ϑ_i . This enables flexible selection of restrictions of the form whether country i 's output depends on country c 's lagged output while turning off dependencies between output in country i and, for instance, lagged interest rates in country c . We set $c_0 = c_1 = 0.01$ and $\vartheta_i = 0.1$. Both hyperparameter values are based on evidence in [Huber and Feldkircher \(2019\)](#), who integrate out ϑ_i in a Bayesian fashion and find values between 0.1 to 0.3, depending on the size of the model involved.

2.5. *Priors for the factor stochastic volatility specification.* For the remaining coefficients we utilize the prior setup proposed in [Kastner \(2019a\)](#). In particular, we use a rowwise NG shrinkage prior on the factor loadings in \mathbf{L} , with its elements denoted by l_{ij} .⁴ We specify the prior

$$l_{ij}|\varphi_{ij}, \zeta_i \sim \mathcal{N}\left(0, \frac{2\varphi_{ij}^2}{\zeta_i}\right), \quad \varphi_{ij}^2 \sim \mathcal{G}(\vartheta_l, \vartheta_l), \quad \zeta_i \sim \mathcal{G}(\epsilon_0, \epsilon_1).$$

The hyperparameters are set to $\vartheta_l = 0.1$ and $\epsilon_0 = \epsilon_1 = 1$. On the parameters of the state equations for the log-volatility processes, we use a normally distributed prior on the unconditional mean $\mu_{\omega_j} \sim \mathcal{N}(0, 10)$ for all j , a Gamma prior on the process innovation variances $\sigma_{s_j}^2 \sim \mathcal{G}(1/2, 1/2)$, and a Beta prior on the (transformed) autoregressive parameter $(\rho_{sj} + 1)/2 \sim \mathcal{B}(10, 3)$ for all s, j . Using different hyperparameter values or estimating the model with weakly informative independent Gaussian priors on the factor loadings has negligible consequences for the results in Section 4.

2.6. *Identification issues.* The model described above is econometrically not identified, with identification issues stemming from two sources. First, the factor model in equation (4) is not identified unless suitable restrictions are introduced. Here, we employ an automatic restriction search approach implemented in [Kastner \(2019b\)](#). The second source arises from the well-known label switching problem.⁵ This issue comes from the invariance of the mixture likelihood function in equation (7) with respect to relabeling the components

$$\begin{aligned} p(\mathbf{c}_i|\mathbf{w}, \boldsymbol{\mu}_1, \dots, \boldsymbol{\mu}_G, \mathbf{V}) &= \sum_{g=1}^G w_g f_{\mathcal{N}}(\mathbf{c}_i|\boldsymbol{\mu}_g, \mathbf{V}) \\ &= \sum_{g=1}^G w_{\varrho(g)} f_{\mathcal{N}}(\mathbf{c}_i|\boldsymbol{\mu}_{\varrho(g)}, \mathbf{V}), \end{aligned}$$

with ϱ indicating a random permutation of $\{1, \dots, G\}$. We obtain identification by applying the random permutation sampler outlined in [Frühwirth-Schnatter \(2001\)](#) and then perform ex post identification of the model. In our case and since N is typically a moderate number of countries, we can easily identify different country groups via economic reasoning. In the empirical application, for instance, we introduce an ordering constraint on the size of the cluster components. Furthermore, notice that if interest centers exclusively on functionals of the coefficients in equation (1), such as impulse response functions or predictive densities, obtaining explicit identification is not necessary. However, it is worth emphasizing that if unbalanced label switching takes place (i.e., the posterior simulator jumps only between a small number of the $G!$ potential modes), inference could be distorted. Using the random permutation sampler in that situation thus leads to balanced label switching, ensuring that the algorithm visits all modes.

This completes the prior setup of our modeling approach. To obtain posterior distributions for all parameters, we propose a Markov chain Monte Carlo (MCMC) algorithm that consists of several blocks. We briefly summarize the algorithm with all full conditional posterior distributions in Appendix A. Moreover, for an illustration of the merits of our approach using synthetic data, see the Supplementary Material ([Huber, Krisztin and Pfarrhofer \(2023\)](#)).

⁴For estimation we rely on the implementation provided in the R-package `factorstochvol` ([Kastner \(2019b\)](#)). Further details on potential variants of the Normal–Gamma shrinkage prior, such as columnwise shrinkage, may be obtained in [Huber and Feldkircher \(2019\)](#).

⁵For a discussion, see [Frühwirth-Schnatter \(2006\)](#).

2.7. Including global variables in our model. Instead of focusing exclusively on country-specific dynamics, we are also interested in how shocks impact a set of L global quantities. In the previous discussion we focused on the case that \mathbf{y}_{it} comprises of the same set of variables and that their treatment is symmetric with respect to the prior setup. In this subsection we discuss how global variables can be incorporated in the general PVAR model.

Suppose that L global variables are included in a vector \mathbf{y}_{0t} . These global variables differ from the ones we use at the country level. In our empirical work, for instance, \mathbf{y}_{0t} captures dynamics on futures markets for energy and agricultural commodities. To capture the effect of \mathbf{y}_{0t} on \mathbf{y}_t (which includes the country-specific information only) we again assume a VAR process,

$$\mathbf{y}_{0t} = \mathbf{A}_{01}\mathbf{y}_{0t-1} + \cdots + \mathbf{A}_{0P}\mathbf{y}_{0t-P} + \mathbf{B}_{01}\mathbf{y}_{t-1} + \cdots + \mathbf{B}_{0P}\mathbf{y}_{t-P} + \boldsymbol{\varepsilon}_{0t}.$$

Here, we let \mathbf{A}_{0j} and \mathbf{B}_{0j} for $j = 1, \dots, P$ denote coefficient matrices of dimension $L \times L$ and $L \times K$, respectively. Notice that all country-specific variables are allowed to impact the global variables. To handle overparameterization concerns, we use a NG shrinkage prior similar to the one described above.

The corresponding country-specific models (for $i = 1, \dots, N$) are slightly modified as follows:

$$(10) \quad \mathbf{y}_{it} = \mathbf{C}_i\mathbf{x}_{it} + \mathbf{B}_i\mathbf{x}_{-i,t} + \mathbf{D}_i\mathbf{z}_t + \boldsymbol{\varepsilon}_{it},$$

whereby \mathbf{D}_i is a $M \times L$ matrix that measures the dynamic relations between \mathbf{y}_{it} and \mathbf{y}_{0t} . In principle, this approach is equivalent to adding \mathbf{y}_{0t} to \mathbf{y}_t but creating a separate cluster that includes only \mathbf{y}_{0t} .

3. Data and model specification. In this section we present a novel dataset to assess the impact of climate shocks on futures markets for agricultural commodities and key macroeconomic quantities across a set of OECD economies.

3.1. Data and descriptive statistics. Our dataset contains monthly observations for 17 OECD member countries, comprised of 13 European member states, Canada, Israel, South Africa, and the U.S. Our sample covers a majority of high-income economies (as defined by the World Bank), accounting for 77% of the population and 82% of output in terms of nominal GDP in U.S. dollars.

The sample includes 215 monthly observations per country, ranging from January 2000 to November 2017. This encompasses multiple major drought and excess rainfall shocks in Europe and the U.S. as well as the food crisis of 2007/08, where the prices of agricultural commodities experienced a sharp peak. The country-specific time series include the consumer price index (CPI), short-term interest rates (IR), the total value of industrial production (IP), and the real effective exchange rate to selected currencies of major trading partners (FX). Movements in food prices are measured through the ratio of the consumer price index for food products to the consumer price index (CPF).⁶

In order to capture the role of the futures market, our dataset includes monthly observations on continuous Chicago Mercantile Exchange (CME) and Intercontinental Exchange (ICE) futures prices with a two-month forward contract for eleven commodities. While the data mainly covers the U.S. futures market, there is strong evidence suggesting that commodity

⁶Our selection of countries is motivated based on our methods requiring a fully balanced monthly panel over an extended time period. Mainly, the joint availability of monthly observation on real effective exchange rates and consumer price indices for food products restricts our sample. Given these constraints, our selection of 17 OECD member countries is as wide as possible for the given time period and variables.

markets are highly integrated, similar to financial markets (e.g., [Cashin, Mohaddes and Raissi \(2017\)](#), [Nazlioglu and Soytas \(2011\)](#), [Huber, Krisztin and Piribauer \(2017\)](#)). This has been emphasized in the literature, especially since the commodity boom in 2004/05. Global shocks to agricultural production are thus expected to be reflected in the U.S. futures market ([Headey \(2011\)](#), [Nazlioglu \(2011\)](#)). Our main crop production measures are rice, corn, cotton, wheat, and soybean futures. Additionally, to assess the role of the livestock sector, we include hogs, feeder, and live cattle futures.⁷ Feeder cattle are freshly weaned calves, whereas live cattle are fully grown animals. The interplay of these two livestock futures allows us to gauge how shocks to feed supply play out in the markets. Moreover, the interlinkages of energy and agricultural markets—specifically, the oil and ethanol markets—is well-established in literature ([Lucotte \(2016\)](#), [Nazlioglu \(2011\)](#), [Nazlioglu and Soytas \(2011\)](#)). To measure the responses of the energy and biofuel sectors to climate shocks, we include crude oil, gas/oil, and ethanol futures in our model. A full list of variables as well as our selection of countries is presented in [Appendix B](#).

Finding a measure, which accurately reflects the presence or absence of climate shocks in agricultural production regions at a national level, poses a serious challenge. National level averages of climate variables, such as precipitation or temperature, fail to take into account the regional variation and localized impact of climate change ([Burke and Tanutama \(2019\)](#), [Harari and Ferrara \(2018\)](#)). To alleviate this issue, we rely on a spatially explicit dataset to proxy climate impacts. This allows us to take the localized nature of climate shocks into account. This data is subsequently aggregated to the supranational level, weighted by a high-resolution dataset of agricultural production. The advantage of this approach is that we explicitly capture localized climate events in high-productivity regions.

Our measure of climate shocks is derived from a drought and excess water availability (which we indicate as flood/excess rainfall) based variable, the Global Standardized Precipitation-Evapotranspiration Index (SPEI), which is a well-established benchmark for capturing joint effects of precipitation, potential evaporation, and temperature ([Beguería et al. \(2014\)](#)).

The SPEI index uses monthly precipitation and potential evapotranspiration data from the CRU weather database as an input variable. The SPEI data is available monthly as a globally gridded dataset, where each pixel has a half-degree resolution. Each monthly observation of the index informs on deviations from the average available water (i.e., the presence and severity of droughts and excess rainfall shocks). Lower values of the index correspond to larger deviations from average water availability conditions, while higher values indicate excess water availability.

Additionally, SPEI data also characterizes the persistence of drought and excess rainfalls, ranging from one to 12 months. In our analysis we focus on persistent droughts and excess rainfalls affecting a substantial share of national agricultural good production. We rely on the index of droughts that are persistent over a time window of three months and that are severe to exceptional ($\text{SPEI} < -1.5$), based on the classification of [Leng and Hall \(2019\)](#). Similarly, as a measure of floods/excessive rainfall we rely on severe to exceptional ($\text{SPEI} > 1.5$) values of the SPEI index over a time window of three months. In the main body of the paper, we focus on a combination of drought and excess rainfall-related shocks, while the [Supplementary Material \(Huber, Krisztin and Pfarrhofer \(2023\)\)](#) contains some additional results for individual shocks.

⁷In all three cases of livestock futures, the actual traded good is the slaughtered, packaged, and frozen meat of the animals.

To quantify the impact of severe to exceptional droughts and excess rainfalls on agricultural production, we combine the SPEI data with spatially explicit data on agricultural production. The spatial production allocation model (SPAM) provides a well-established baseline of gridded, global agricultural production areas at a 5-arcminute resolution in the year 2000. The data was obtained by harmonizing subnational and national production statistics with satellite-based remote sensing data (Balkovič et al. (2014)). SPAM provides growing area information on a wide range of crop types with varying degrees of accuracy. Due to data limitations and to provide robustness for our assessment, we focus on the main crop types corn, rice, maize, and wheat, which jointly cover 75% of the caloric content of global food production (Roberts and Schlenker (2013)). Observations on average yields in kilocalories per hectare under different levels of crop management intensification are obtained from the biophysical EPIC model (van der Velde et al. (2012)).⁸ Combining data on crop production areas and yields provides us with a gridded dataset of potential production in kilocalories at a half-degree level.

Drought and excess rainfall-related events are assumed to only have an impact during growing season which differs substantially by production regions. We use the AQUASTAT crop calendar to inform us on worldwide growing seasons. We aggregate the percent of monthly kilocaloric crop production for 11 supranational regions (see Appendix B for a definition of the climatic regions) which is subject to severe or exceptional droughts and excess rainfalls lasting for three or more months during growing season.

Figure 1 displays the resulting climate shock index. The black line and grey areas show the impact of droughts and excess rainfalls in percent of caloric production per region. Inspection of regional results reveals that trends in annual yield shortfalls are captured well by the index. Particularly well-known severe drought events, such as the drought in the U.S. in 2012/13 or in Australia (located in the OCE group) in 2007/08 are clearly visible. The index also picks up other climate-related stylized facts, such as the higher incidence of droughts and extreme climate events in the Middle East and North Africa (MNA), Sub-Saharan Africa (SSA) and Southeast Asia (SAS).

Figure 2 displays the correlation of drought and excess rainfall-related shocks among regions across our sample. Note that both drought and the combination of drought and excess rainfall-related shocks exhibit spatial correlation, with geographically close regions being correlated more strongly. This is particularly evident in the drought shocks (left panel), where the strongest correlations are among regions with similar latitude (e.g., OCE and LAC or USA and CAN). A similar pattern, albeit somewhat muted, can be observed in the combined drought and excess rainfall shocks (right panel), where the strongest correlations are between USA and EUR as well as EUR and CAN regions.

3.2. Model specification. We use the model outlined in Section 2. In particular, the variables included in the vector of global futures market quantities y_{0t} and the country-specific macroeconomic time series in y_{it} are

$$\begin{aligned} y_{0t} &= (\text{Crudeoil, Gas/Oil, Corn, Rice, Soya, Soybean Oil, Wheat, Cotton, Ethanol, } \dots \\ &\quad \text{Hogs, Cattle (F), Cattle (L)})', \\ y_{it} &= (\text{CPI, CPF, IR, IP, FX})'. \end{aligned}$$

We introduce climate shocks for aggregate regions through the exogenous scalar time series r_{jt} (for $j = 1, \dots, \mathcal{J}$, where j marks a specific region) to assess the contemporaneous

⁸The EPIC model simulates potential crop growth under various biophysical and management conditions, which we transform by using FAO conversion values from tons per hectare for each of our main crops.

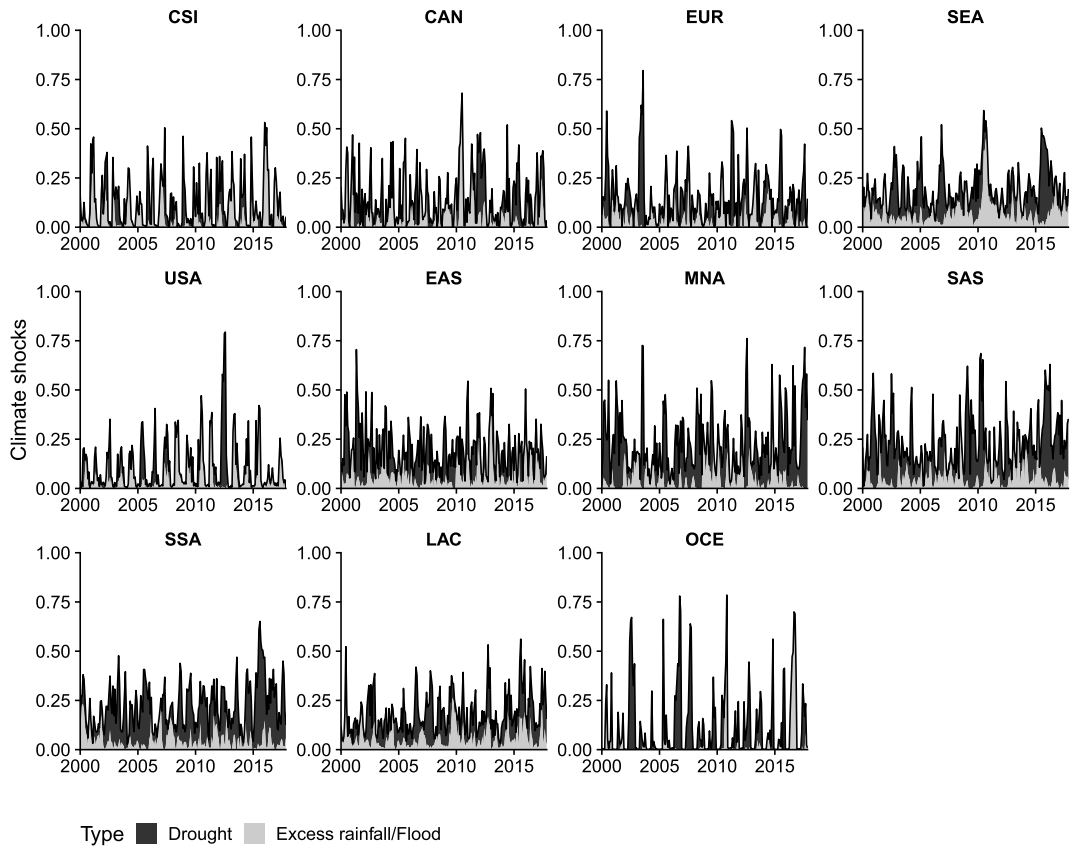


FIG. 1. Percent of caloric production under severe exceptional three-month drought and excess rainfall/flood (grey shaded areas) and their sum (black line).

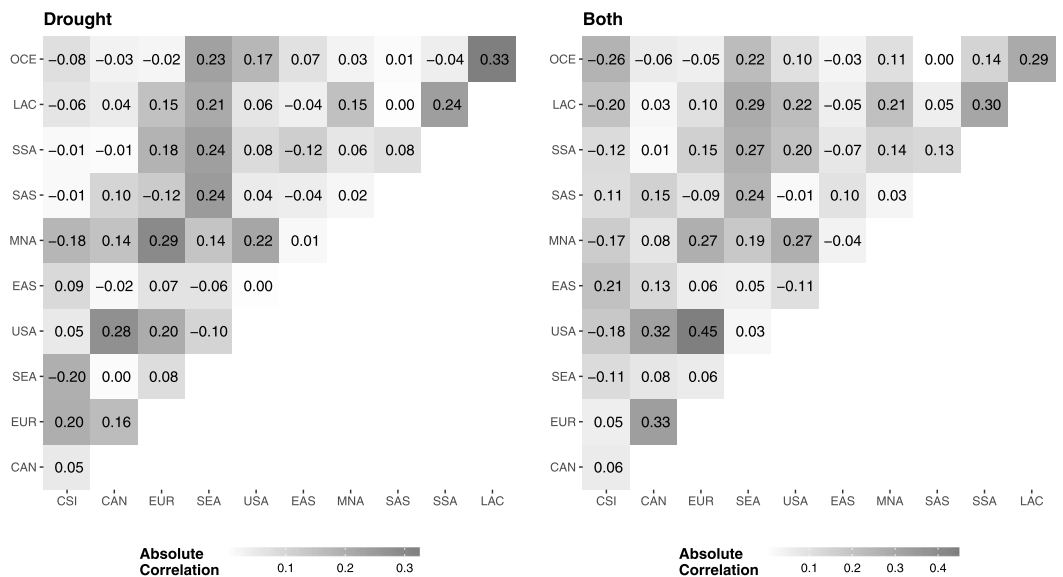


FIG. 2. Region-by-region correlations of climate shocks series for drought and drought/excess rainfall. The regions are ordered by the latitude coordinates of their centroids.

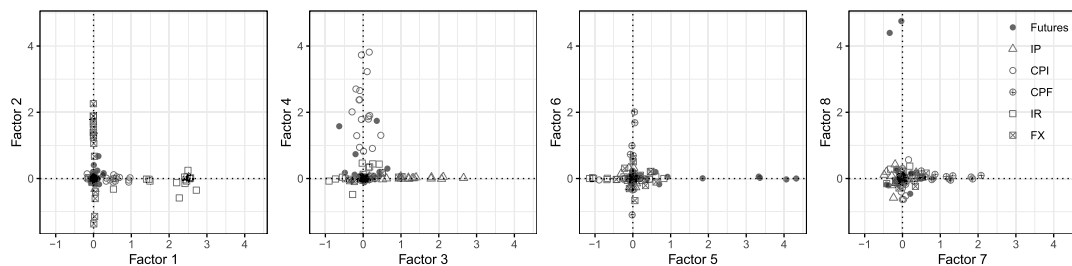


FIG. 3. Pairwise scatterplots of the posterior median loadings by variable type across latent factors.

The third factor tracks joint movements in industrial production across economies. Turning to factors shaping the error structure of commodities futures prices, we find the highest factor loadings for the second, fourth, and fifth factors. Interestingly, the second factor appears to also drive the shocks for exchange rates, providing a link between foreign exchange rate and commodity markets. The fourth factor governs contemporaneous dynamics of commodities futures markets and consumer price inflation across economies, while the fifth factor shows the largest loadings for futures prices in terms of the respective magnitude of the loadings. Notice that the eighth latent factor mostly shows loadings close to zero, providing further evidence that this number is likely sufficient to capture dynamics in the variance-covariance structure of the model.

In the following discussion we focus on three factors associated with the largest loadings on futures market prices. Figure 4 plots the full history of the log volatilities over the sample period. The volatilities with the highest loadings on commodity futures highlight multiple stylized facts. First, the peak of the volatilities in 2008 in all three plots coincides with the global financial crisis. However, note that fifth factor also reflects the so-called food price crisis, where food and energy commodities rose sharply, with associated increased volatility (Headey (2011)). Additionally, the sharp increase in commodity futures volatilities in 2013 corresponds to severe droughts impacting the U.S. It should be pointed out that the magnitude of volatilities differs sharply across the factors, with the fourth factor—most strongly associated with CPI and commodity futures—exhibiting the largest values. Commodity futures are in fact seen as a possible hedge against inflation, providing an explanation for the shared volatility structure.

Moreover, for the sake of completeness, we present some evidence on series specific idiosyncrasies for commodities futures prices in Figure 5. A few points are worth noting here. First, we again find substantial differences in the magnitude of the volatilities across series. Second, evidence for time variation in the idiosyncratic components of the error terms is muted for soybeans and soyoil, while we find substantial movements in the idiosyncratic log volatilities for the remaining series. Specifically, we do not find evidence for an increase in the idiosyncratic log volatilities of biofuels during the stock market and food price crisis of

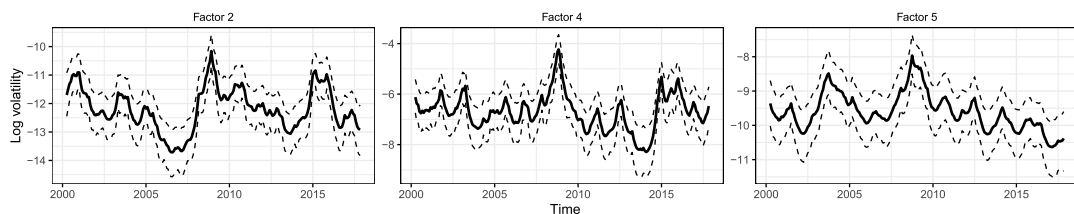


FIG. 4. Log volatilities of the factors with largest loadings for commodities futures prices. The solid black line indicates the posterior median, while dashed lines refer to the 16th and 84th percentiles of the posterior distribution.

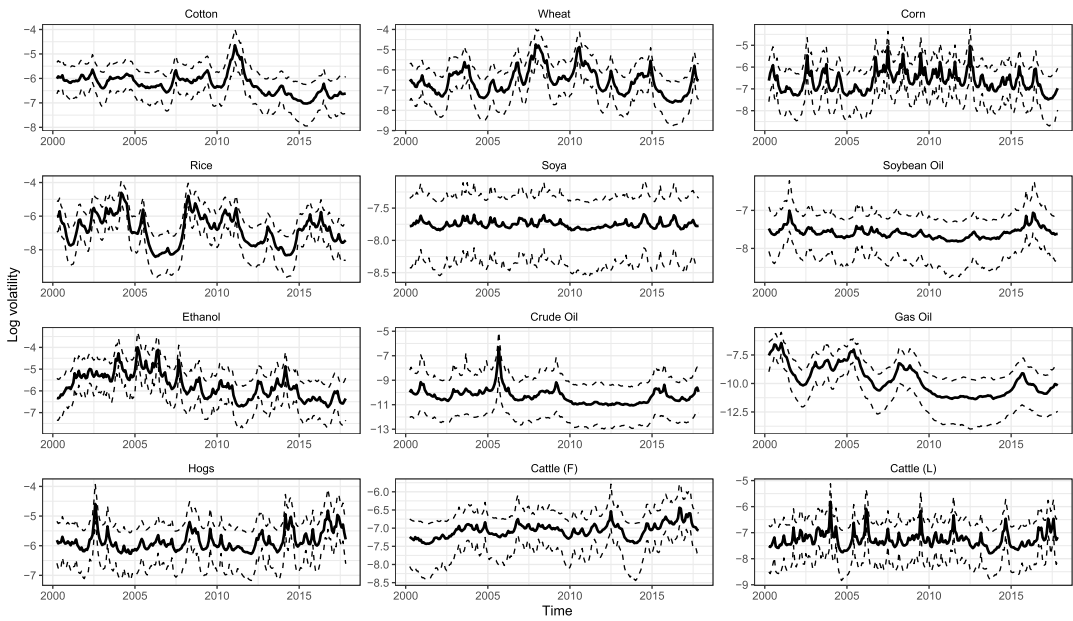


FIG. 5. *Idiosyncratic log volatility components of commodities futures prices. The solid black line indicates the posterior median, while dashed lines refer to the 16th and 84th percentiles of the posterior distribution.*

2008/09. This implies that, while energy and agricultural futures clearly share similar volatility patterns, the link is not necessarily provided by biofuel markets and related U.S. policy (Nazlioglu and Soytaş (2011)).

The idiosyncratic log volatilities of crude oil and gas/oil exhibit similar patterns, especially after the global financial crisis. The 2015 volatility spike, which is largely due to supply side consolidation, especially of shale oil companies, can clearly be observed. The log volatilities of corn exhibit seasonal patterns. These represent a well-known fact of the U.S. corn futures market and are connected to corn stock movements. Moreover, the 2013 drought, evident in Figure 1, is reflected as the highest volatility spike in corn futures.

Closer inspection of idiosyncratic livestock log volatility patterns reveals that live cattle and hogs closely track the volatilities of crop markets as feeder cattle. This reflects the fact that both of these livestock futures relate to animals which have to reach full maturity and are tightly linked to global feed prices. Note that some pronounced volatility spikes in corn, cotton, and ethanol futures are tracked with a slight delay by the hogs and live cattle markets, due to these crops being a major food source for hogs and cattles. The increase in the log volatilities of the livestock market since 2016 can be clearly observed. Initially, changing CME futures market regulations were blamed for this increase; however, the trend has persisted. Since then, despite regulatory countermeasures, the causes are subject of ongoing research.

The impact of climate shocks on global futures prices. In the following we consider the impact of climate-related drought/excess rainfall shocks on financial markets. The empirical literature emphasizes spillovers from energy to agricultural markets as causal effects for rising food prices (Baumeister and Peersman (2013), Lucotte (2016), Nazlioglu and Soytaş (2011)). The dynamic responses of a wide range of commodity futures to regionally located climate shocks provide evidence on the prevalence of strong linkages between global commodity prices and an increase in drought and excess rainfall events.

Figure 6 summarizes the peak endogenous responses to exogenous drought/excess rainfall shocks across multiple geographic areas, measured in percent of potential kilocaloric produc-

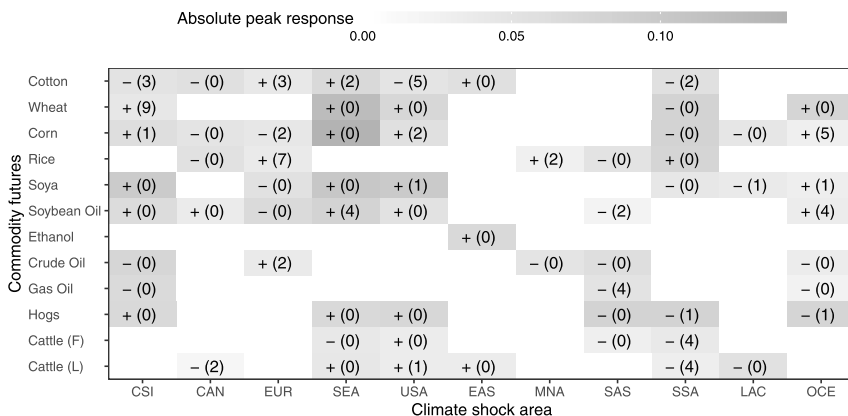


FIG. 6. Peak impulse response (excess rainfall and drought shocks) for commodities futures prices. The shading indicates the absolute magnitude of the response. Plus/minus refers to the direction of the response; the numbers in parentheses are months after the impact of the shock when the peak response occurs. Insignificant impulse responses, based on the 16th and 84th percentiles of the posterior distribution covering zero, are left blank.

tion under severe drought/excess rainfall, in a single plot. Additional results and robustness checks are provided in the Supplementary Material (Huber, Krisztin and Pfarrhofer (2023)). The shading indicates the absolute magnitude of the response. Plus/minus refers to the direction of the response, while the numbers in parentheses are months after the impact of the shock when the peak response occurs. Insignificant impulse responses, that is, responses where the 16th and 84th percentiles of the posterior distribution cover zero, are displayed as blank.

The responses underlying Figure 6 are illustrated for both types of shocks—the sum of drought/excess rainfall and only drought shocks in the U.S.—in Figure 7.⁹ The grey shaded areas correspond to 68th percentile credible intervals. Combined drought/excess rainfall shocks correspond to the dash-dot line, while the dashed line denotes a drought shock only. The futures for the agricultural products corn, soybeans, and wheat are the three most valuable crops in terms of their aggregate production value in the U.S.

A first and rough inspection of the figures reveals that drought and excess rainfall shocks can induce both positive and negative reactions in the futures markets. Positive responses can be interpreted as a direct result of tightening agricultural supply. Negative reactions may stem from various causes.

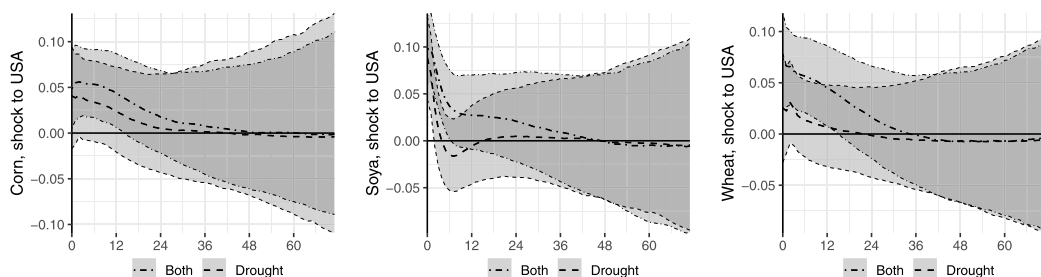


FIG. 7. Impulse responses of corn, soybeans, and wheat commodities futures to climate shocks in the U.S. Shaded areas refer to 68 percent posterior credible set. “Both” denotes combined drought/excess rainfall shock, while “Drought” denotes only a drought shock.

⁹Additional empirical results are available in the Supplementary Material (Huber, Krisztin and Pfarrhofer (2023)). The full set of impulse response functions across shock regions and economies is available upon request.

Zooming into the precise results, a few observations stand out. First and foremost, a short-term (within a couple of months) decrease in prices might be interpreted as the overshooting behavior of agricultural commodity prices. Second, a medium term decrease in prices could indicate agricultural production shifting to crops that are less affected by adverse climate effects, for example, crops with lower water demand or higher resilience to climate volatility. A further prevalent explanation for a price decrease are supply chain effects, such as droughts and excess rainfall damage causing a decrease in demand for livestock feed and associated products. The literature suggests that these effects play a key role in lower-income regions, such as Sub-Saharan Africa, where wide-spread subsistence level farming coupled with climate change leads to lower demand for imported agricultural goods for feed-related purposes (Amare et al. (2018), Minot (2014)). Finally, a medium- to long-term decrease in commodity prices might be caused by production shifting to producing regions not affected by the climate shock or where higher yields can be obtained.

In the case of combined drought and excess rainfall shocks in the U.S., our results suggest that all considered crop and livestock futures, with the exception of rice and cotton, exhibit a positive price response, peaking in the relative short-term of zero to two months. This is also evident in the impulse response functions in Figure 7. Note that in the case of a drought shock, only soybeans exhibit a significant price increase. A potential explanation could be the high ratio of irrigable cropland which can mitigate the effect of drought on agricultural production. The price of cotton decreases, albeit only slightly in the medium term. This could be interpreted as a substitution effect. Particularly, cotton is seen as a competitor for soy and corn production—both of which are seen as less resilient to climatic impacts.

Former U.S.S.R. countries have been a major producer and consumer of soybeans prior to the collapse of large-scale production in the late 1990s. As a result, Russia and Western Asian (CSI) countries are now major importers of soybeans and have started expanding production again only in the last decade (Headey (2011)). Therefore, a drought shock translates to a sharp increase of prices in global soy markets, as is evident in our results. Moreover, combined drought and excess rainfall shocks lead to a short-term increase in corn prices and a longer term increase (peak at nine months) of wheat price futures. The delayed peak is likely the result of wheat stocks. The dip in cotton prices mirrors the responses in the U.S. in magnitude and is likely also due to substitution effects. The significant decrease in global oil futures prices is likely due to droughts being coupled with higher temperatures which can significantly lower heating costs in cold climate regions.

The peak impulse response functions for Canada (CAN) are relatively muted. This is likely due to the fact that Canada is not a major agriculture producing region and drought/excess rainfall shocks have only minor impacts. The short-term price decreases of crops, followed by a dip in life cattle, could be interpreted as the climate shocks affecting cattle production and causing a dip in feed prices. The increase in soybean oil prices indicates an excess demand for biofuels, of which Canada is a major global producer.

The peak impulse responses to a drought/excess rainfall shock in Europe (EUR) suggests an increase in rice and cotton prices, coupled with an increase in crude oil prices peaking after two months. This, together with a decrease in corn, soybean, and soyoil futures, suggests that these crops and associated products are more robust to climatic shocks and yields might also increase as a result of excess rainfall (Urban et al. (2015)). The increase in crude oil futures peaking after two months can be interpreted as mitigation efforts by agricultural producers.

Southeast Asia (SEA) presents an interesting case, as it experienced major expansions of palm oil plantations, used both in fuel production and as biofuels, to the detriment of cropland and pastures in the recent decade. This is reflected in our results by a sharp increase in corn, wheat, soy, and livestock prices in response to a climate shock. Feeder cattle prices exhibit an immediate dip, likely due to producers faced with increasing feeder prices flooding the market with young cattle for immediate meat production.

Our results for the major producing region of Eastern Asia (EAS), encompassing China, Japan, and South Korea, underline the effects of a drought/excess rainfall shocks on cotton and cattle prices. Note also that the climate impacts lead to an immediate increase in ethanol futures prices, where China is one of the leading producer regions.

Turning our attention to the results of drought/excess rainfall shocks in the Middle East and North Africa (MNA), we provide evidence of sharp increases in rice prices. This is related to the shocks impacting domestic production.

Considering the results for droughts/excess rainfall in Southern Asia (SAS), we find decreases in prices across a wide range of futures. Since the region itself encompasses developing economies with a low per capita income but a large share of global production, this provides support of a change in demand in relatively poorer countries as a result of climate shocks (Amare et al. (2018), Minot (2014)). The persistent dip in oil prices is evidence of the major role of transportation costs: a shortfall of exports leads to less demand for fuel (Headey (2011)).

For shocks in Sub-Saharan Africa (SSA), our results suggest a decrease in cotton, wheat, corn, soybean, hogs, and livestock prices, coupled with an increase in the global futures price for rice. Household level surveys, such as Minot (2014) and Amare et al. (2018), provide evidence for a drop in demand for multiple imported goods, due to a decrease in household income, which is supported by our results. While SSA accounts for only two percent of global rice production, they are a major per capita consumer of rice products, and the majority of local production is also consumed locally (Headey (2011)). Thus, a drought shock turns into increased imports and, in turn, an increase in global prices.

A drought/excess rainfall-related shock to agricultural production areas in Latin American countries (LAC) leads to an immediate dip in corn, soybeans, and live cattle futures prices. The joint dip in major feed and live cattle prices suggests that futures markets react to the climate shock by selling live cattle which causes a subsequent dip in feed prices. Additionally, climate-related shocks, especially in South and Central America, are thought to lead to a conversion of cropland areas into pastures (Headey (2011)) which, in turn, increases global supply of livestock products.

Drought shocks in Oceania (OCE), covering the high output economies New Zealand and Australia, yield similar responses as in Europe. The shortfall in domestic production leads to excess demand and a sharp increase in global wheat, corn, soybean, and soyoil prices. These price spikes are persistent and in the case of soybean, rice and corn, peak only after four months. Lean hogs futures prices decrease, likely due to producers selling early to avoid increased production costs. The decrease in global oil prices points to a decrease in exports.

Impacts on high-income economies. In order to obtain a more detailed picture of how global drought/excess rainfall shocks play out in high-income economies, we now consider the country-specific results of our model for several key macroeconomic series.

Figure 8 displays peak responses to exogenous climate shocks for a set of macroeconomic variables in a single plot. Each subpanel of the figure contains peak responses for all drought/excess rainfall shocks in the 11 global climatic regions. The shading corresponds to the absolute magnitude of the response, while the plus/minus signs indicate the direction of the response. The numbers in parentheses denote the peak of the response after the impact of the shock in months. Insignificant impulse responses (under the 16th and 84th percentile) are again displayed as blank.

Selected nonaggregated, individual impulse responses, which Figure 8 is based upon, are presented for a climate shock in the U.S. in Figure 9. Additional results are provided in the Supplementary Material (Huber, Krisztin and Pfarrhofer (2023)). The plot contains the response of selected variables (IP, CPF, IR, and XR) for the U.S., Canada, Japan, and the

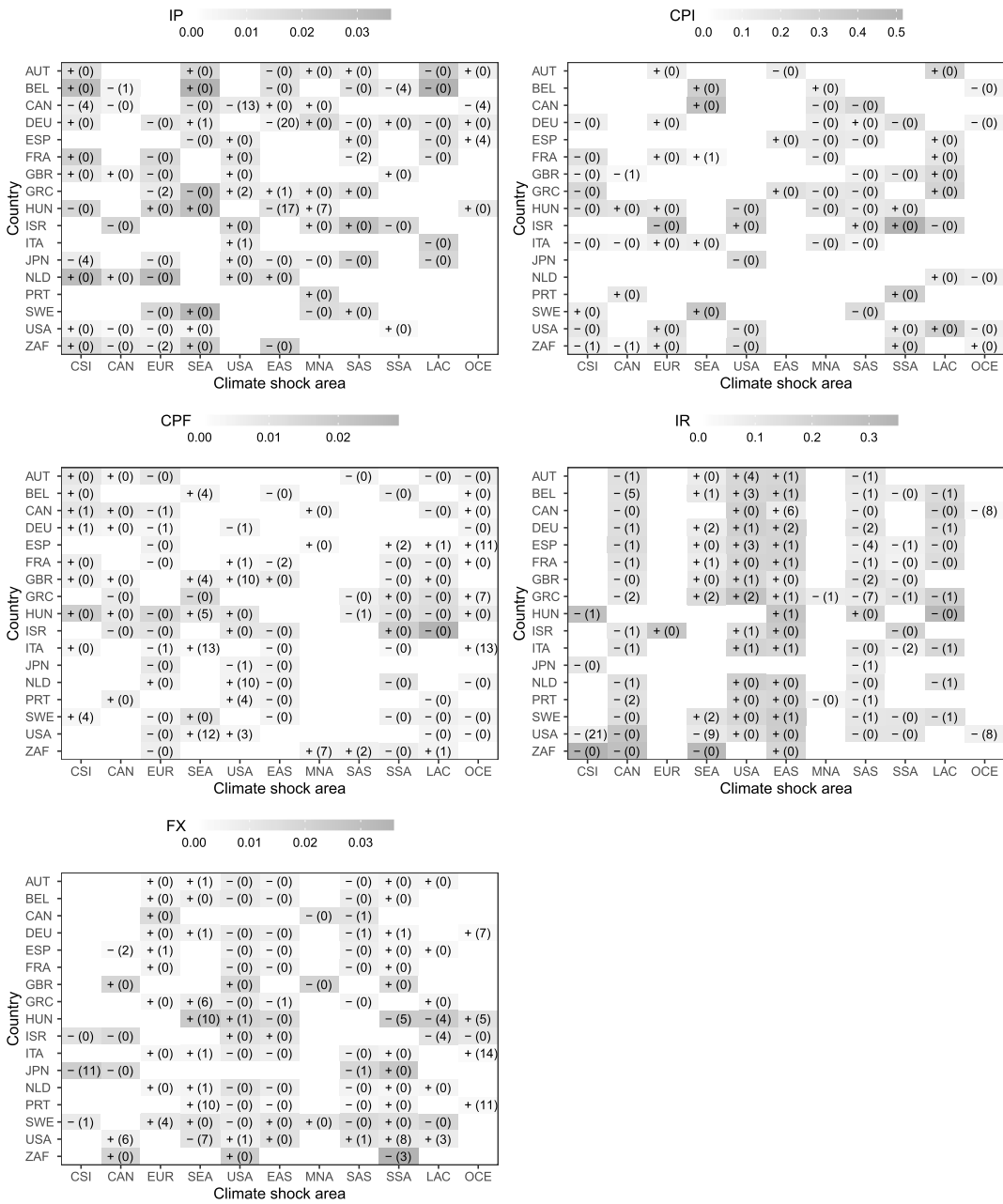


FIG. 8. Peak impulse responses (excess rainfall and drought shocks) across countries and variable types. The shading indicates the absolute magnitude of the response; plus/minus refers to the direction of the response, while the numbers in parentheses are months after the impact of the shock when the peak response occurs. Insignificant impulse responses, based on the 16th and 84th percentiles of the posterior distribution covering zero, are left blank.

U.K. These countries were the largest (in 2010 USD) users/importers of U.S. agricultural trade goods in our study period. The figure illustrates both drought/excess rainfall (dash-dot line) as well as drought shocks in isolation (dashed line), while the grey shaded areas indicate 68% credible intervals.

A first inspection of Figures 8 and 9 reveals that droughts and excess rainfall events indeed exhibit spillovers on price changes, interest rates, and economic output. The magnitude, direction, and significance of these shocks is dependent on a countries' overall dependence

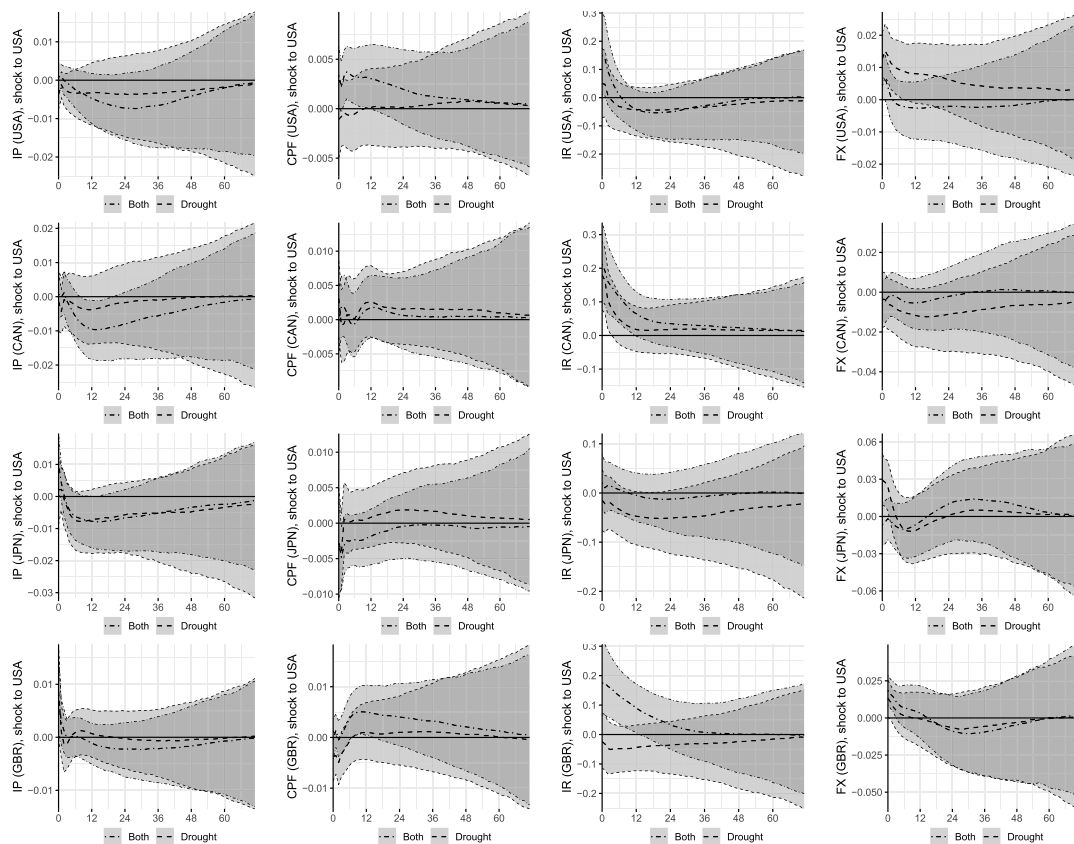


FIG. 9. Impulse responses of selected variables to a shock (excess rainfall and drought) in the U.S. Shaded areas refer to 68% posterior credible set.

on agricultural goods as well as geographic proximity and trade ties to the drought/excess rainfall impacted climatic region. Nonetheless, some regularities can be readily observed. Exchange and interest rate responses of Euro area countries exhibit comovements, due to the common monetary policy. Additionally, the responses of interest rates display significant comovement across the sample. The direction of this comovement seems to strongly depend on which climatic region is impacted by the shocks. This can be explained by the fact that the countries of interest represent developed economies with homogeneous choices of trading partners amongst the eleven climatic regions (Baker et al. (2018)).

The magnitude of food price responses are rather muted, as compared to the aggregate change in CPI. While this might seem surprising, the pronounced response in short-term interest rates can be seen as a compensation of shocks that would otherwise increase food prices. This is supported by recent literature documenting the relationship of CPF and interest rates which views interest rates as implicitly mitigating climate shocks (Akram (2009), de Nicola, De Pace and Hernandez (2016)). Finally, it is worth mentioning that the peak responses manifest within the first months in countries that were directly impacted by the drought/excess rainfall shock. Spillover to other countries typically are seen later on.

While an exogenous drought/excess rainfall shock in the U.S. has only modest domestic effects, our results provide evidence for spillovers to other regions. Canada (in monetary terms the largest importer of U.S. agricultural goods) exhibits a dip in industrial production, peaking a year after the shock. Multiple European economies as well as Japan and Israel exhibit an immediate increase in industrial production as a response to a climate shock in the U.S. Moreover, a climate shock in the U.S. increases food prices around three months after

the shock in several of the considered economies. Spillover effects on average food prices in other regions vary in intensity, with the most pronounced responses being in the U.K. and Netherlands. Relatedly, we observe a minor increase of the real effective exchange rate of the U.S. dollar which is consistent with the U.S. being a large importer of food stocks. This indicates that the shortfall of production is matched by imports. Interestingly, the exchange rate of Canada—the largest trading partner of the U.S.—does not change significantly, reflecting that agricultural commodities are imported from elsewhere. However, Canada experiences a short decrease in inflation which is matched by a decrease in interest rates consistent with expansionary monetary policy counteracting disinflationary pressures. The real effective exchange rates of almost all Euro area economies and Israel exhibit a slight dip, coupled with decreases in short-term interest rates and a one to five month spike in output. This indicates a direct increase in production to cover the U.S. shortfalls. The responses in inflation are mixed, pointing to a slight short-term increase in Sweden, Portugal and Greece.

The impacts of a drought/excess rainfall shock in Russia and Western Asia (CSI) are characterized by a reduction of short-term interest rates, combined with short-term food price and output spikes in major trading partners. Note that positive impacts on production are short-term in most European countries. This is closely related to our findings that drought shocks in the CSI region induce a dip in crude oil and gas/oil prices (Lucotte (2016)).

Focusing on the domestic response to a drought/excess rainfall shock in Canada (CAN), we observe that food prices experience a short spike, where food prices exceed average prices by over one percent initially. This is matched by a decrease in interest rates and a statistically significant decline in industrial production. Canada's largest trading partner, the U.S., exhibits similar patterns, albeit without increases in relative food prices. Price and output fluctuations can be observed throughout the European economies around the first months, reflecting adjustments to the economy to a drought shock in a large ethanol producing country. Major importers of Canadian products, such as the U.K., also experience spike in food prices directly following the climate shock.

The real effective exchange rate responses to a drought/excess rainfall shock in Europe (EUR) provide evidence that all European economies (with the exception of the United Kingdom, Hungary, and Portugal) significantly increase imports to match the shortfalls in agricultural production. The responses in output within Europe are mixed, with the majority of countries experiencing a decrease in production, with the exception of Austria, Italy, Hungary, Portugal, and Spain. Note that food prices decrease across all European countries with the exception of the Netherlands. The responses in the U.S. to a European drought shock demonstrate an increase in exports, coupled with an initial drop in production. This phenomenon occurs at the same time as global futures prices for wheat and rice increase, pointing to shortages in food availability as a possible explanation.

A climate shock in Southeast Asia (SEA) results in the strongest responses in industrial production across our sample of economies. In most cases the response is an immediate increase in industrial production, with the exception of Spain and Greece where production dips modestly. The shocks result in a CPF increase over the medium- to long-term (four to 13 months). This is consistent with a supply shocks to agricultural production. Note that the drought/excess rainfall shocks also yield increases in interest rates, mostly coinciding with the food price increases. The real effective exchange rates also tend to increase.

Examining drought/excess rainfall shocks in Eastern Asia (EAS), we observe that Japan, and some parts of Europe face a shortfall in production and a negative reaction of output. The results highlight that countries such as the U.S., Austria, Germany, Hungary, and South Africa experience a small delayed (after a horizon of 12 to 20 months), albeit significant, decrease in industrial production. This might be an indication of the overshooting behavior of commodity markets, since many of these countries expand their production in response to the climate shock in Asia.

Droughts and excess rainfall events in Middle East and Northern Africa (MNA) cause a significant, albeit small, positive reaction on output and a dip in inflation in almost all economies under consideration. The results from a drought/excess rainfall shock in Sub-Saharan Africa (SSA) have relatively muted effects on industrial production, causing only a short-term dip in Israel and Belgium. The effect of the shock on prices and interest rates is limited, except for Israel where the climate shock leads to a spike in inflation with a relative increase in food prices and a decrease in short-term interest rates. This may be explained by noting that Israel has substantial agricultural import ties with Sub-Saharan Africa. Almost all countries in our sample exhibit a statistically significant increase in real effective exchange rates in response to a climate shock which is consistent with increased imports. South Africa is not significantly affected in terms of output or exchange rate fluctuations. This underlines findings of [Amare et al. \(2018\)](#) who argue that demand shifts due to droughts are only in effect in lower-income countries, as opposed to high-income economies.

The peak impulse responses to a climate change shock in Latin America (LAC) indicate a negative impact on interest rates across almost all countries of the sample, accompanied by a short period of declines in output. This reflects the large contribution of Latin American countries to crop and livestock production globally ([Headey \(2011\)](#)). Major trading partners like the U.S. and some European countries increase imports. Additionally, across the Euro area food prices relative to overall price levels dip significantly after the shock.

5. Concluding remarks. In this paper we focus on the highly policy relevant question of assessing the impacts and transmission channels of climate change shocks on a set of high-income OECD economies. For this purpose we measure climate change-related shocks using a novel index measuring the percentage of agricultural production under severe, persistent drought, and excess rainfall, constructed by using spatially explicit datasets. Moreover, we specifically focus on macroeconomic quantities, such as output, interest and exchange rates as well as food prices and inflation. Moreover, our approach controls for the crucial role of global commodity markets in the agricultural sector. In order to efficiently cope with the large number of variables, we develop a PVAR model that pools information across countries using a sparse finite mixture of Gaussians prior on the domestic, country-specific coefficients. We control for the existence of dynamic interdependencies by relying on a global-local shrinkage prior to stochastically select nonzero relationships across countries and variable types. Static interdependencies are parsimoniously modeled through a factor stochastic volatility specification of the error variance-covariance matrix.

Our findings suggest that climate shocks have a sizable effect on global commodity markets as well as on country-specific macroeconomic variables. The strongest effects can be found for interest rates and inflation, consistent with U.S.-based studies such as [Akram \(2009\)](#) and [Cashin, Mohaddes and Raissi \(2017\)](#). The quantitative relevance of climate shocks points toward substantial policy implications. For instance, higher frequencies and intensities of climate shocks triggered by climate change require appropriate fiscal and monetary policies to mitigate the economic implications of climate change. Major central banks, such as the European Central Bank, now explicitly analyze and discuss appropriate policy reactions to climate change in recent strategy reviews ([Drudi et al. \(2021\)](#)). Our results contribute to this discussion by providing quantitative guidance on how climate shocks impact financial markets and the wider macroeconomy.

Additionally, we provide evidence for climate change impacts on high-income countries, even if the associated events manifest in a different part of the world. The global commodity market results corroborate the findings of [Nazlioglu and Soytaş \(2012\)](#) and [Lucotte \(2016\)](#), who also find strong evidence for the interdependence between energy and agricultural markets coupled with an increased global demand for biofuels.

APPENDIX A: POSTERIOR SIMULATION

- (1) Simulation of VAR coefficients, factor loadings, and stochastic volatility components:
 - (a) Sample \mathbf{A}_i and \mathbf{B}_i from their Gaussian conditional posterior distributions on an equation-by-equation basis. Conditional on $\mathbf{L}\mathbf{f}_t$, the conditional posterior for each equation of equation (1) is given by

$$\begin{pmatrix} [\mathbf{C}_i]_{j\bullet}' \\ [\mathbf{B}_i]_{j\bullet}' \end{pmatrix} | \bullet \sim \mathcal{N}(\bar{\mathbf{c}}_{ij}, \bar{\mathbf{M}}_{ij})$$

for $i = 1, \dots, N$ and $j = 1, \dots, M$. The posterior mean and variance are given by

$$\begin{aligned} \bar{\mathbf{M}}_{ij} &= (\tilde{\mathbf{X}}_i' \tilde{\mathbf{X}}_i + \mathbf{W}_i^{-1})^{-1}, \\ \bar{\mathbf{c}}_{ij} &= \bar{\mathbf{M}}_{ij} (\tilde{\mathbf{X}}_i' [\tilde{\mathbf{Y}}_i]_{\bullet j} + \mathbf{W}_i^{-1} \boldsymbol{\psi}_{ij}) \end{aligned}$$

with $\tilde{\mathbf{X}}_i$ being a full-data matrix with typical t th row, given by $(\mathbf{x}'_{it}, \mathbf{x}'_{-i,t}) \exp(-\omega_{in}/2)$. The index n selects the element of $\boldsymbol{\Omega}_t$ associated with the j th equation in country i and $[\tilde{\mathbf{Y}}_i]_{\bullet j}$ has typical element $y_{ij,t} - [\mathbf{L}]_{n\bullet} \mathbf{f}_t$. In addition, $\mathbf{W}_i = \text{diag}(\mathbf{V}_j, \boldsymbol{\Delta}_{ij})$ with $\boldsymbol{\Delta}_{ij}$ being a diagonal prior variance-covariance matrix for the j th equation constructed using equation (9), and $\boldsymbol{\psi}_{ij}$ is a prior mean matrix that consists of the elements in $\boldsymbol{\mu}_g$ associated with the j th equation, for $\delta_i = g$, and the remaining elements are set equal to zero. The matrix \mathbf{V}_j is constructed by selecting the variance parameters in \mathbf{V} that relate to the j th equation.

- (b) We simulate the quantities related to the factor stochastic volatility specification using the R-package `factorstochvol` (Kastner (2019b)). Details on the posterior quantities involved are presented in Kastner (2019a). Specifically, the algorithm draws first the full history of the idiosyncratic volatilities h_{jt} , the volatilities of the factors ω_{jt} , and the corresponding parameters $\phi_{\omega j}$, ρ_{sj} and σ_{sj} . The subsequent step produces draws for the global and local shrinkage parameters from the rowwise Normal–Gamma prior specification. In the next step, simple Bayesian regression updates can be used to obtain a draw for the factor loadings matrix \mathbf{L} . To speed up mixing in this step, the algorithm relies on deep interweaving techniques. The final updating step produces a draw for the full history of the factors \mathbf{f}_t .
- (2) Simulation of quantities associated with the mixture model:
 - (a) Sample the mixture probabilities \mathbf{w} from a Dirichlet distribution, given by

$$\mathbf{w} | \bullet \sim \text{Dir}(p_1, \dots, p_G),$$

with $p_g = p_0 + N_g$ and $N_g = \#\{i : \delta_i = g\}$ denoting the number of countries located in cluster g .

- (b) The regime measures δ_i are simulated from a multinomial distribution with

$$\Pr(\delta_i = k) \propto w_k f_{\mathcal{N}}(\mathbf{c}_i | \boldsymbol{\mu}_g, \mathbf{V}).$$

- (c) We obtain draws for the group-specific means from a multivariate Gaussian distribution,

$$\begin{aligned} \boldsymbol{\mu}_g | \bullet &\sim \mathcal{N}(\bar{\boldsymbol{\mu}}_g, \bar{\mathbf{V}}_g), \\ \bar{\mathbf{V}}_g &= (N_g \mathbf{V}^{-1} + \mathbf{Q}_0^{-1})^{-1}, \\ \bar{\boldsymbol{\mu}}_g &= \bar{\mathbf{V}}_g (N_g \mathbf{V}^{-1} \bar{\mathbf{c}}_g + \mathbf{Q}_0^{-1} \boldsymbol{\mu}_0). \end{aligned}$$

$\bar{\mathbf{c}}_g = \frac{\sum_{i=1}^N \mathbf{c}_i \delta_i}{N_g}$ denotes the mean of the domestic quantities associated with group g .

- (d) The common variance-covariance matrix V is obtained by independently sampling v_j ($j = 1, \dots, m$) from

$$v_j | \bullet \sim \mathcal{G}^{-1} \left(w_0 + \frac{N}{2}, w_1 + \frac{\sum_{n=1}^N (c_{nj} - \mu_{nj})^2}{2} \right),$$

where $\mu_{nj} = \mu_{gj}$ if $\delta_n = g$.

- (e) We simulate λ_j from a generalized inverted Gaussian (GIG) distribution,¹⁰

$$\lambda_j | \bullet \sim \mathcal{GIG}(p_G, d_j, e_j).$$

After simulating all λ_j s we construct $Q_0 = \Lambda R_0 \Lambda$, with R_0 being based on the most recent Gibbs draw of c .

- (f) The full conditional posterior of μ_0 is Gaussian with

$$\mu_0 | \bullet \sim \mathcal{N}(\bar{\mu}_0, \bar{Q}_0),$$

whereby $\bar{\mu}_0 = \frac{1}{G} \sum_{g=1}^G \mu_g$ and $\bar{Q}_0 = \frac{1}{G} Q_0$.

- (g) Simulate the intensity parameter of the Dirichlet prior p_0 using a random walk Metropolis–Hastings algorithm on the log scale. The full conditional posterior density of p_0 is given by

$$p(p_0 | \mathbf{w}) \propto p(\mathbf{w} | p_0) p(p_0).$$

We propose a value p_0^* from $p_0^* \sim p_0^{(a)} e^z$ with $z \sim \mathcal{N}(0, c)$. Here, we let c be a tuning parameter specified such that the acceptance rate lies between 20 and 40% and $p_0^{(a)}$ denotes the last accepted draw. The probability of accepting a new draw is then

$$\alpha(p_0^*, p_0^{(a)}) = \min \left[\frac{p(\mathbf{w} | p_0^*) p(p_0^*) p_0^{(a)}}{p(\mathbf{w} | p_0^{(a)}) p(p_0^{(a)}) p_0^*}, 1 \right].$$

- (3) Simulation of shrinkage parameters on dynamic interdependencies:

- (a) For each country $i = 1, \dots, N$, simulate the global shrinkage parameters ξ_i from a Gamma distribution,

$$\xi_i | \bullet \sim \mathcal{G} \left(c_0 + \vartheta_i k, c_0 + \frac{\vartheta_i}{2} \sum_{i=1}^k \tau_{ij} \right).$$

- (b) Sample the local shrinkage parameters from their GIG distributed posteriors

$$\tau_{ij} | \bullet \sim \mathcal{GIG} \left(\vartheta_i - \frac{1}{2}, \vartheta_i \xi_i, b_{ij}^2 \right)$$

for $i = 1, \dots, N$ and $j = 1, \dots, k$.

- (4) Apply a random permutation step by simulating one of $G!$ possible permutations of $\{1, \dots, G\}$, labeled ϱ ,

$$(w_1, \dots, w_G)' = (w_{\varrho(1)}, \dots, w_{\varrho(G)}),$$

$$(\mu_1, \dots, \mu_G)' = (\mu_{\varrho(1)}, \dots, \mu_{\varrho(G)}),$$

$$\delta = \varrho(\delta).$$

In case we include a set of global variables (such as in our empirical work), the corresponding coefficients can be estimated in precisely the same way as the ones for the country-specific variables.

APPENDIX B: REGIONS AND DATA

TABLE 2

Composition of aggregated global climatic regions and the associated countries

Canada (CAN)	Europe (EUR)	Middle-East and	Burkina Faso
Canada	Romania	North-Africa (MNA)	Sub-Saharan Africa
Russia and West Asia	Serbia and Montenegro	Lebanon	(SSA)
(CSI)	Slovakia	Libya	Burundi
Armenia	Slovenia	Morocco	Cameroon
Azerbaijan	Spain	Oman	Cape Verde
Belarus	Sweden	Qatar	Central African Republic
Georgia	Switzerland	Saudi Arabia	Chad
Kazakhstan	United Kingdom	Syria	Comoros
Kyrgyzstan	Latin America (LAC)	Tunisia	Congo
Moldova	Argentina	Turkey	Congo DR
Russian Federation	Bahamas	United Arab Emirates	Cote d'Ivoire
Tajikistan	Belize	Western Sahara	Djibouti
Turkmenistan	Bolivia	Yemen	Equatorial Guinea
Ukraine	Brazil	Oceania (OCE)	Eritrea
Uzbekistan	Chile	Australia	Ethiopia
East Asia (EAS)	Colombia	Fiji	Gabon
China	Costa Rica	French Polynesia	Gambia
Japan	Cuba	New Caledonia	Ghana
Republic of Korea	Dominican Republic	New Zealand	Guinea
Europe (EUR)	Ecuador	Papua New Guinea	Guinea-Bissau
Albania	El Salvador	Samoa	Kenya
Austria	Falkland Islands	Solomon Islands	Lesotho
Belgium	French Guiana	Vanuatu	Liberia
Bosnia and Herzegovina	Guadeloupe	South Asia (SAS)	Madagascar
Bulgaria	Guatemala	Bangladesh	Malawi
Croatia	Guyana	Bhutan	Mali
Cyprus	Haiti	India	Mauritania
Czech Republic	Honduras	Nepal	Mauritius
Denmark	Jamaica	Pakistan	Mozambique
Estonia	Mexico	Sri Lanka	Namibia
Finland	Nicaragua	Southeast Asia (SEA)	Niger
France	Panama	Brunei Darussalam	Nigeria
Germany	Paraguay	Cambodia	Reunion
Greece	Peru	Indonesia	Rwanda
Greenland	Suriname	Korea DPR	Senegal
Hungary	Trinidad and Tobago	Laos	Sierra Leone
Iceland	Uruguay	Malaysia	Somalia
Ireland	Venezuela	Mongolia	South Africa
Italy	Middle-East and	Myanmar	Sudan
Latvia	North-Africa (MNA)	Philippines	Swaziland
Lithuania	Algeria	Singapore	Tanzania
Luxembourg	Bahrain	Thailand	Togo
Macedonia	Egypt	Viet Nam	Uganda
Malta	Iran	Sub-Saharan Africa	Zambia
Netherlands	Iraq	(SSA)	Zimbabwe
Norway	Israel	Angola	United States of
Poland	Jordan	Benin	America (USA)
Portugal	Kuwait	Botswana	United States of America

TABLE 3
Abbreviations and variable descriptions of the PVAR information set and sources of the data

Futures prices (Abbreviation)	Description and source
Crude oil	Intercontinental Exchange Brent Crude Futures, Continuous Contract #2 (Source: <i>Quandl/CHRIS</i>)
Gas/Oil	Intercontinental Exchange Gas Oil Futures, Continuous Contract #2 (Source: <i>Quandl/CHRIS</i>)
Corn	Chicago Mercantile Exchange Corn Futures, Continuous Contract #2 (Source: <i>Quandl/CHRIS</i>)
Rice	Chicago Mercantile Exchange Rough Rice Futures, Continuous Contract #2 (Source: <i>Quandl/CHRIS</i>)
Soya	Chicago Mercantile Exchange Soya Futures, Continuous Contract #2 (Source: <i>Quandl/CHRIS</i>)
Soybean Oil	Chicago Mercantile Exchange Soybean Oil Futures, Continuous Contract #2 (Source: <i>Quandl/CHRIS</i>)
Wheat	Chicago Mercantile Exchange Wheat Futures, Continuous Contract #2 (Source: <i>Quandl/CHRIS</i>)
Cotton	Intercontinental Exchange Cotton No. 2 Futures, Continuous Contract #2 (Source: <i>Quandl/CHRIS</i>)
Ethanol	Chicago Mercantile Exchange Ethanol Futures, Continuous Contract #2 (Source: <i>Quandl/CHRIS</i>)
Hogs	Chicago Mercantile Exchange Lean Hogs Futures, Continuous Contract #2 (Source: <i>Quandl/CHRIS</i>)
Cattle (F)	Chicago Mercantile Exchange Feeder Cattle Futures, Continuous Contract #2 (Source: <i>Quandl/CHRIS</i>)
Cattle (L)	Chicago Mercantile Exchange Live Cattle Futures, Continuous Contract #2 (Source: <i>Quandl/CHRIS</i>)
Macroeconomic variables (Abbreviation)	Description and source
CPI	Nominal seasonally adjusted consumer price index, measured in log differences. (Source: <i>World Bank</i>)
CPF	Ratio of nominal, seasonally adjusted food consumer price index and CPI, measured in log levels. (Source: <i>FAO</i>)
IR	Short term interest rates, percent per annum, measured in log levels. (Source: <i>OECD</i>)
IP	Total value of industrial production, in seasonally adjusted 2010 USD, measured in log levels. (Source: <i>World Bank</i>)
FX	Real effective exchange rate index, measured in log levels. (Source: <i>World Bank</i>)

Acknowledgments. This paper is a substantially revised version of a manuscript titled “Dealing with cross-country heterogeneity in panel VARs using finite mixture models.”

Funding. The authors gratefully acknowledge financial support from the Oesterreichische Nationalbank (Jubilaeumsfond grant no. 17650), the Austrian Science Fund (FWF): ZK 35, the European Union’s Horizon 2020 research and innovation programme under grant agreements No 776479 and No 820712.

¹⁰We assume that x follows a GIG distribution if its density is proportional to $x^{a-1} \exp\{-(bx + c/x)/2\}$ with $a \in \mathbb{R}$ and $b, c > 0$.

SUPPLEMENTARY MATERIAL

Additional empirical results. (DOI: [10.1214/22-AOAS1681SUPPA](https://doi.org/10.1214/22-AOAS1681SUPPA); .zip). This section collects several additional results. These include impulse responses to drought shocks only and cross-sectionally aggregated impulse responses. Individual responses across countries and shock-regions are available upon request.

Simulation based evidence (DOI: [10.1214/22-AOAS1681SUPPB](https://doi.org/10.1214/22-AOAS1681SUPPB); .pdf). In this section we evaluate the merits of our approach by means of an extensive simulation exercise.

REFERENCES

- AGUILAR, O. and WEST, M. (2000). Bayesian dynamic factor models and portfolio allocation. *J. Bus. Econom. Statist.* **18** 338–357.
- AKRAM, Q. F. (2009). Commodity prices, interest rates and the dollar. *Energy Econ.* **31** 838–851. <https://doi.org/10.1016/j.eneco.2009.05.016>
- ALESSANDRI, P. and MUMTAZ, H. (2021). The macroeconomic cost of climate volatility. Preprint. Available at [arXiv:2108.01617](https://arxiv.org/abs/2108.01617).
- ALLENBY, G. M., ARORA, N. and GINTER, J. L. (1998). On the heterogeneity of demand. *J. Mark. Res.* **35** 384–389.
- AMARE, M., JENSEN, N. D., SHIFERAW, B. and CISSÉ, J. D. (2018). Rainfall shocks and agricultural productivity: Implication for rural household consumption. *Agric. Syst.* **166** 79–89. <https://doi.org/10.1016/j.agsy.2018.07.014>
- BAFFES, J. and HANIOTIS, T. (2010). Placing the recent commodity boom into perspective. In *Food Prices and Rural Poverty* 40–70. World Bank, Washington DC.
- BAI, J. and NG, S. (2007). Determining the number of primitive shocks in factor models. *J. Bus. Econom. Statist.* **25** 52–60. MR2338870 <https://doi.org/10.1198/073500106000000413>
- BAKER, J., HAVLIK, P., BEACH, R., LECLÈRE, D., SCHMID, E., VALIN, H., COLE, J., CREASON, J., OHREL, S. et al. (2018). Evaluating the effects of climate change on US agricultural systems: Sensitivity to regional impact and trade expansion scenarios. *Environ. Res. Lett.* **13** 1–48.
- BALKOVIČ, J., VAN DER VELDE, M., SKALSKÝ, R., XIONG, W., FOLBERTH, C., Khabarov, N., SMIRNOV, A., MUELLER, N. D. and OBERSTEINER, M. (2014). Global wheat production potentials and management flexibility under the representative concentration pathways. *Glob. Planet. Change* **122** 107–121. <https://doi.org/10.1016/j.gloplacha.2014.08.010>
- BAUMEISTER, C. and PEERSMAN, G. (2013). The role of time-varying price elasticities in accounting for volatility changes in the crude oil market. *J. Appl. Econometrics* **28** 1087–1109. MR3137716 <https://doi.org/10.1002/jae.2283>
- BEGUERÍA, S., VICENTE-SERRANO, S. M., REIG, F. and LATORRE, B. (2014). Standardized Precipitation Evapotranspiration Index (SPEI) revisited: Parameter fitting, evapotranspiration models, tools, datasets and drought monitoring. *Int. J. Climatol.* **34** 3001–3023.
- BHATTACHARYA, A., PATI, D., PILLAI, N. S. and DUNSON, D. B. (2015). Dirichlet–Laplace priors for optimal shrinkage. *J. Amer. Statist. Assoc.* **110** 1479–1490. MR3449048 <https://doi.org/10.1080/01621459.2014.960967>
- BURKE, M. and TANUTAMA, V. (2019). Climatic constraints on aggregate economic output. *NBER Working Paper* **25779**.
- CANOVA, F. and CICCARELLI, M. (2004). Forecasting and turning point predictions in a Bayesian panel VAR model. *J. Econometrics* **120** 327–359. MR2058892 [https://doi.org/10.1016/S0304-4076\(03\)00216-1](https://doi.org/10.1016/S0304-4076(03)00216-1)
- CANOVA, F. and CICCARELLI, M. (2009). Estimating multicountry VAR models. *Internat. Econom. Rev.* **50** 929–959. MR2542805 <https://doi.org/10.1111/j.1468-2354.2009.00554.x>
- CANOVA, F. and CICCARELLI, M. (2013). Panel vector autoregressive models: A survey. In *VAR Models in Macroeconomics—New Developments and Applications: Essays in Honor of Christopher A. Sims. Adv. Econom.* **32** 205–246. Emerald Group Publ. Ltd., Bingley. MR3496837 <https://doi.org/10.1108/S0731-905320130000031006>
- CARRIERO, A., CLARK, T. E. and MARCELLINO, M. (2019). Large Bayesian vector autoregressions with stochastic volatility and non-conjugate priors. *J. Econometrics* **212** 137–154. MR3994011 <https://doi.org/10.1016/j.jeconom.2019.04.024>
- CASHIN, P., MOHADDES, K. and RAISSI, M. (2017). Fair weather or foul? The macroeconomic effects of El Niño. *J. Int. Econ.* **106** 37–54.

- CHAN, J., EISENSTAT, E. and YU, X. (2022). Large Bayesian VARs with factor stochastic volatility: Identification, order invariance and structural analysis. *arXiv:2207.03988*.
- CRESPO CUARESMA, J., FELDKIRCHER, M. and HUBER, F. (2016). Forecasting with global vector autoregressive models: A Bayesian approach. *J. Appl. Econometrics* **31** 1371–1391. MR3580905 <https://doi.org/10.1002/jae.2504>
- DE NICOLA, F., DE PACE, P. and HERNANDEZ, M. A. (2016). Co-movement of major energy, agricultural, and food commodity price returns: A time-series assessment. *Energy Econ.* **57** 28–41. <https://doi.org/10.1016/j.eneco.2016.04.012>
- DEES, S., DI MAURO, F., PESARAN, M. H. and SMITH, L. V. (2007). Exploring the international linkages of the Euro area: A global VAR analysis. *J. Appl. Econometrics* **22** 1–38. MR2359200 <https://doi.org/10.1002/jae.932>
- DOAN, T. R., LITTERMAN, B. R. and SIMS, C. A. (1984). Forecasting and conditional projection using realistic prior distributions. *Econometric Rev.* **3** 1–100.
- DRUDI, F., MOENCH, E., HOLTHAUSEN, C., WEBER, P.-F., FERRUCCI, G., SETZER, R., NINO, V. D., BARBIERO, F., FACCIA, D. et al. (2021). Climate change and monetary policy in the euro area.
- ELLER, M., HUBER, F. and SCHUBERTH, H. (2020). How important are global factors for understanding the dynamics of international capital flows? *J. Int. Money Financ.* **109** 102221.
- ENDERS, W. and HOLT, M. T. (2014). *The Evolving Relationships Between Agricultural and Energy Commodity Prices: A Shifting-Mean Vector Autoregressive Analysis*. Univ. Chicago Press, Chicago.
- FAO (2017). *The Future of Food and Agriculture: Trends and Challenges*. FAO, Rome.
- FELDKIRCHER, M. and HUBER, F. (2016). The international transmission of US shocks? evidence from Bayesian global vector autoregressions. *Eur. Econ. Rev.* **81** 167–188.
- FELDKIRCHER, M., HUBER, F., KOOP, G. and PFARRHOFER, M. (2022). Approximate Bayesian inference and forecasting in huge-dimensional multicountry VARs. *Internat. Econom. Rev.* forthcoming. <https://doi.org/10.1111/iere.12577>
- FRÜHWIRTH-SCHNATTER, S. (2001). Markov chain Monte Carlo estimation of classical and dynamic switching and mixture models. *J. Amer. Statist. Assoc.* **96** 194–209. MR1952732 <https://doi.org/10.1198/016214501750333063>
- FRÜHWIRTH-SCHNATTER, S. (2006). *Finite Mixture and Markov Switching Models*. Springer Series in Statistics. Springer, New York. MR2265601
- FRÜHWIRTH-SCHNATTER, S. (2011). Dealing with label switching under model uncertainty. In *Mixtures: Estimation and Applications*. Wiley Ser. Probab. Stat. 213–239. Wiley, Chichester. MR2883354 <https://doi.org/10.1002/9781119995678.ch10>
- FRÜHWIRTH-SCHNATTER, S. and KAUFMANN, S. (2008). Model-based clustering of multiple time series. *J. Bus. Econom. Statist.* **26** 78–89. MR2422063 <https://doi.org/10.1198/073500107000000106>
- FRÜHWIRTH-SCHNATTER, S., TÜCHLER, R. and OTTER, T. (2004). Bayesian analysis of the heterogeneity model. *J. Bus. Econom. Statist.* **22** 2–15. MR2028204 <https://doi.org/10.1198/073500103288619331>
- GARCIA, P., IRWIN, S. H. and SMITH, A. (2015). Futures market failure? *Am. J. Agric. Econ.* **97** 40–64. <https://doi.org/10.1093/ajae/aa067>
- GAUPP, F., PFLUG, G., HOCHRAINER-STIGLER, S., HALL, J. and DADSON, S. (2017). Dependency of crop production between global breadbaskets: A copula approach for the assessment of global and regional risk pools. *Risk Anal.* **37** 2212–2228. <https://doi.org/10.1111/risa.12761>
- GEORGIADIS, G. (2015). Examining asymmetries in the transmission of monetary policy in the euro area: Evidence from a mixed cross-section global VAR model. *Eur. Econ. Rev.* **75** 195–215.
- GILBERT, C. L. (2010). How to understand high food prices. *J. Agric. Econ.* **61** 398–425. <https://doi.org/10.1111/j.1477-9552.2010.00248.x>
- GRIFFIN, J. E. and BROWN, P. J. (2010). Inference with normal-gamma prior distributions in regression problems. *Bayesian Anal.* **5** 171–188. MR2596440 <https://doi.org/10.1214/10-BA507>
- GUERRERO, S., HERNÁNDEZ-DEL VALLE, G. and JUÁREZ-TORRES, M. (2017). Using a functional approach to test trending volatility in the price of Mexican and international agricultural products. *J. Agric. Econ.* **48** 3–13. <https://doi.org/10.1111/agec.12290>
- HARARI, M. and FERRARA, E. L. (2018). Conflict, climate and cells: A disaggregated analysis. *Rev. Econ. Stat.* **100** 594–608.
- HARRI, A., NALLEY, L. and HUDSON, D. (2009). The relationship between oil, exchange rates, and commodity prices. *Journal of Agricultural and Applied Economics* **41** 501–510. <https://doi.org/10.1017/S1074070800002959>
- HAUZENBERGER, N., HUBER, F., KOOP, G. and ONORANTE, L. (2021). Fast and flexible Bayesian inference in time-varying parameter regression models. *J. Bus. Econom. Statist.* 1–15.
- HAVLÍK, P., SCHNEIDER, U. A., SCHMID, E., BÖTTCHER, H., FRITZ, S., SKALSKÝ, R., AOKI, K., CARA, S. D., KINDERMANN, G. et al. (2011). Global land-use implications of first and second generation biofuel targets. *Energy Policy* **39** 5690–5702. <https://doi.org/10.1016/j.enpol.2010.03.030>

- HEADEY, D. (2011). Rethinking the global food crisis: The role of trade shocks. *Food Policy* **36** 136–146. <https://doi.org/10.1016/j.foodpol.2010.10.003>
- HIRSCH, C., KRISZTIN, T. and SEE, L. (2020). Water resources as determinants for foreign direct investments in land—a gravity analysis of foreign land acquisitions. *Ecol. Econ.* **170** 106516.
- HUANG, H., VON LAMPE, M. and VAN TONGEREN, F. (2011). Climate change and trade in agriculture. *Food Policy* **36** S9–S13. <https://doi.org/10.1016/j.foodpol.2010.10.008>
- HUBER, F. (2016). Density forecasting using Bayesian global vector autoregressions with stochastic volatility. *Int. J. Forecast.* **32** 818–837.
- HUBER, F. and FELDKIRCHER, M. (2019). Adaptive shrinkage in Bayesian vector autoregressive models. *J. Bus. Econom. Statist.* **37** 27–39. MR3910223 <https://doi.org/10.1080/07350015.2016.1256217>
- HUBER, F., KRISZTIN, T. and PFARRHOFER, M. (2023). Supplement to “A Bayesian panel vector autoregression to analyze the impact of climate shocks on high-income economies.” <https://doi.org/10.1214/22-AOAS1681SUPPA>, <https://doi.org/10.1214/22-AOAS1681SUPPB>
- HUBER, F., KRISZTIN, T. and PIRIBAUER, P. (2017). Forecasting global equity indices using large Bayesian vars. *Bull. Econ. Res.* **69** 288–308. MR3680268 <https://doi.org/10.1111/boer.12094>
- IFPRI (2008). *High Food Prices: The What, Who, and How of Proposed Policy Actions*. IFPRI, Washington DC.
- ISHWARAN, H., JAMES, L. F. and SUN, J. (2001). Bayesian model selection in finite mixtures by marginal density decompositions. *J. Amer. Statist. Assoc.* **96** 1316–1332. MR1946579 <https://doi.org/10.1198/016214501753382255>
- JANSENS, C., HAVLÍK, P., KRISZTIN, T., BAKER, J., FRANK, S., HASEGAWA, T., LECLÈRE, D., OHREL, S., RAGNAUTH, S. et al. (2020). Global hunger and climate change adaptation through international trade. *Nat. Clim. Change* **10** 829–835.
- JAROCIŃSKI, M. (2010). Responses to monetary policy shocks in the East and the West of Europe: A comparison. *J. Appl. Econometrics* **25** 833–868. MR2756988 <https://doi.org/10.1002/jae.1082>
- JEBABLI, I., AROURI, M. and TEULON, F. (2014). On the effects of world stock market and oil price shocks on food prices: An empirical investigation based on TVP-VAR models with stochastic volatility. *Energy Econ.* **45** 66–98. <https://doi.org/10.1016/j.eneco.2014.06.008>
- KASTNER, G. (2019a). Sparse Bayesian time-varying covariance estimation in many dimensions. *J. Econometrics* **210** 98–115. MR3944765 <https://doi.org/10.1016/j.jeconom.2018.11.007>
- KASTNER, G. (2019b). `factorstochvol`: Bayesian Estimation of (Sparse) Latent Factor Stochastic Volatility Models. R-package version 0.9.
- KASTNER, G. and HUBER, F. (2020). Sparse Bayesian vector autoregressions in huge dimensions. *J. Forecast.* **39** 1142–1165. MR4161021 <https://doi.org/10.1002/for.2680>
- KIM, H. S., MATTHES, C. and PHAN, T. (2021). Extreme Weather and the Macroeconomy. Available at SSRN 3918533.
- KOOP, G. and KOROBILIS, D. (2016). Model uncertainty in panel vector autoregressive models. *Eur. Econ. Rev.* **81** 115–131.
- KOOP, G. and KOROBILIS, D. (2018). Forecasting with high-dimensional panel VARs. *Essex Finance Centre Working Papers* **31**.
- KOROBILIS, D. (2016). Prior selection for panel vector autoregressions. *Comput. Statist. Data Anal.* **101** 110–120. MR3504839 <https://doi.org/10.1016/j.csda.2016.02.011>
- LENG, G. and HALL, J. (2019). Crop yield sensitivity of global major agricultural countries to droughts and the projected changes in the future. *Science of the Total Environment* **654** 811–821. <https://doi.org/10.1016/j.scitotenv.2018.10.434>
- LENK, P. J. and DESARBO, W. S. (2000). Bayesian inference for finite mixtures of generalized linear models with random effects. *Psychometrika* **65** 93–119.
- LUCOTTE, Y. (2016). Co-movements between crude oil and food prices: A post-commodity boom perspective. *Econom. Lett.* **147** 142–147. MR3552172 <https://doi.org/10.1016/j.econlet.2016.08.032>
- MALSINER-WALLI, G., FRÜHWIRTH-SCHNATTER, S. and GRÜN, B. (2016). Model-based clustering based on sparse finite Gaussian mixtures. *Stat. Comput.* **26** 303–324. MR3439375 <https://doi.org/10.1007/s11222-014-9500-2>
- MINOT, N. (2014). Food price volatility in sub-Saharan Africa: Has it really increased? *Food Policy* **45** 45–56. <https://doi.org/10.1016/j.foodpol.2013.12.008>
- MIRANDA-AGRIPPINO, S. and REY, H. (2020). U.S. monetary policy and the global financial cycle. *Rev. Econ. Stud.* **87** 2754–2776. MR4170663 <https://doi.org/10.1093/restud/rdaa019>
- NAZLIOGLU, S. (2011). World oil and agricultural commodity prices: Evidence from nonlinear causality. *Energy Policy* **39** 2935–2943. <https://doi.org/10.1016/j.enpol.2011.03.001>
- NAZLIOGLU, S. and SOYTAS, U. (2011). World oil prices and agricultural commodity prices: Evidence from an emerging market. *Energy Economics* **33** 488–496. <https://doi.org/10.1016/j.eneco.2010.11.012>

- NAZLIOGLU, S. and SOYTAS, U. (2012). Oil price, agricultural commodity prices, and the dollar: A panel cointegration and causality analysis. *Energy Economics* **34** 1098–1104. <https://doi.org/10.1016/j.eneco.2011.09.008>
- PARK, T. and CASELLA, G. (2008). The Bayesian lasso. *J. Amer. Statist. Assoc.* **103** 681–686. MR2524001 <https://doi.org/10.1198/016214508000000337>
- PESARAN, M. H., SCHUERMANN, T. and WEINER, S. M. (2004). Modeling regional interdependencies using a global error-correcting macroeconomic model. *J. Bus. Econom. Statist.* **22** 129–181. MR2041460 <https://doi.org/10.1198/073500104000000019>
- PITT, M. K. and SHEPHARD, N. (1999). Time-varying covariances: A factor stochastic volatility approach. In *Bayesian Statistics, 6 (Alcoceber, 1998)* 547–570. Oxford Univ. Press, New York. MR1724873
- PUMA, M. J., BOSE, S., CHON, S. Y. and COOK, B. I. (2015). Assessing the evolving fragility of the global food system. *Environmental Research Letters* **10**. <https://doi.org/10.1088/1748-9326/10/2/024007>
- ROBERTS, M. J. and SCHLENKER, W. (2013). Identifying supply and demand elasticities of agricultural commodities: Implications for the US ethanol mandate. *American Economic Review* **103** 2265–2295.
- ROUSSEAU, J. and MENGENSEN, K. (2011). Asymptotic behaviour of the posterior distribution in overfitted mixture models. *J. R. Stat. Soc. Ser. B Stat. Methodol.* **73** 689–710. MR2867454 <https://doi.org/10.1111/j.1467-9868.2011.00781.x>
- SAGHAIAN, S. H. (2010). The impact of the oil sector on commodity prices: Correlation or causation? *Journal of Agricultural and Applied Economics* **42** 477–485. <https://doi.org/10.1017/S1074070800003667>
- SANDSTRÖM, V., VALIN, H., KRISZTIN, T., HAVLÍK, P., HERRERO, M. and KASTNER, T. (2018). The role of trade in the greenhouse gas footprints of EU diets. *Global Food Security* **19** 48–55. <https://doi.org/10.1016/j.gfs.2018.08.007>
- SERRA, T., ZILBERMAN, D., GIL, J. M. and GOODWIN, B. K. (2011). Nonlinearities in the U.S. corn-ethanol-oil-gasoline price system. *Agricultural Economics* **42** 35–45. <https://doi.org/10.1111/j.1574-0862.2010.00464.x>
- URBAN, D. W., ROBERTS, M. J., SCHLENKER, W. and LOBELL, D. B. (2015). The effects of extremely wet planting conditions on maize and soybean yields. *Climatic Change* **130** 247–260.
- VAN HUELLEN, S. (2018). How financial investment distorts food prices: Evidence from U.S. grain markets. *Agricultural Economics* **49** 171–181. <https://doi.org/10.1111/agec.12406>
- VAN DER VELDE, M., TUBIELLO, F. N., VRIELING, A. and BOURAOUI, F. (2012). Impacts of extreme weather on wheat and maize in France: Evaluating regional crop simulations against observed data. *Climatic Change* **113** 751–765. <https://doi.org/10.1007/s10584-011-0368-2>
- YAU, C. and HOLMES, C. (2011). Hierarchical Bayesian nonparametric mixture models for clustering with variable relevance determination. *Bayesian Anal.* **6** 329–351. MR2806247 <https://doi.org/10.1214/11-BA612>